# Wave propagation in a periodically modulated low-pass transmission line

by

**José Roberto Reyes Ayona**
**M.Sc., INAOE**

A Dissertation Submitted to the Program in Electronics Science, Electronics Science Department in partial fulfillment of the requirements for the degree of

DOCTOR OF SCIENCES
WITH THE SPECIALTY IN ELECTRONICS

at the

National Institute for Astrophysics, Optics and Electronics
June 2015,
Tonantzintla, Puebla

Advisor:

Prof. Peter Halevi
Electronics Department, INAOE

# Abstract

Wave propagation in transmission lines has been the subject of study for many decades. In a transmission line, waves of different frequencies propagate with different velocities and different wavelengths. The relation between the phase advance of a wave and its frequency is given by the dispersion relation $\omega(\beta)$. A transmission line can have spatial or temporal periodicity. For a spatially periodic transmission line the dispersion relation displays phase advance periodicity and frequency gaps whilst for a temporally periodic transmission line the dispersion relation presents phase advance gaps and frequency periodicity. A dynamic medium is one in which at least one of the characteristics that define it changes with time. A dynamic medium with periodic permittivity $\varepsilon(t)$ is periodic in $\omega$ and there are forbidden bands for the phase advance $\beta$. When a monochromatic plane wave of frequency $\omega$ is incident on such a medium, the reflected and transmitted waves contain harmonics of the modulation frequency $\Omega$. Transmission lines are spatially periodic and are widely used to transport voltage signals. In this thesis, a transmission line with spatial and temporal periodicity and with a new modulation method is presented. The temporal periodicity is given by time-changing capacitors (varactors). A realistic model to describe this dynamic transmission line (DTL) is proposed. This model considers losses, voltage modulation effects and no linearity of varactors. A general solution for the dispersion relation is found and solved for different parameters of the DTL. An approximate solution that gives insight on DTLs performance is also found. It is proved that a DTL can be described as an effective medium for the long wavelength limit [$C(t)/a = \varepsilon(t)$, $L/a = \mu$, and $\beta a << 1$]. Experimental verification and comparison with theoretical results were made, the results include dispersion relations, harmonic generation and frequency beats.

# Resumen

La propagación de ondas en líneas de transmisión se ha estudiado durante muchas décadas. En una línea de transmisión ondas de diferentes frecuencias se propagan con diferentes velocidades. La forma en que se relaciona una frecuencia y se avance de fase está descrita por la relación de dispersión $\omega(\beta)$. La relación de dispersión de una línea de transmisión muestra periodicidad en el avance de fase y bandas prohibidas en frecuencia para la periodicidad espacial, y periodicidad en la frecuencia y bandas prohibidas en el avance de fase para la periodicidad temporal. Un medio dinámico es aquel en el cual al menos una de las características que lo definen cambia con el tiempo. Un medio dinámico con permitividad periódica $\varepsilon(t)$ es periódico en $\omega$ y presenta bandas prohibidas para el avance de fase $\beta$. Cuando una onda monocromática plana incide en ese tipo de medio, las ondas reflejadas y transmitidas contienen armónicos de la frecuencia de modulación $\Omega$. Las líneas de transmisión tienen periodicidad espacial y son ampliamente usadas para transportas señales de voltaje. En esta tesis se presenta a una línea de transmisión con periodicidad espacial y temporal, la cual se modula con un nuevo enfoque. La periodicidad temporal de esta línea se obtiene por medio de capacitores variables en el tiempo (varactores). Se propone un modelo realista para describir a esta línea, el modelo considera pérdidas, los efectos del voltaje de modulación y la no linealidad de los varactores. Se encuentra una solución general para la relación de dispersión y luego se resuelve para diferentes parámetros de la línea. También se encuentra una solución aproximada la cual da una perspectiva del funcionamiento de la línea. Se prueba que esta línea puede ser descrita a través de un medio efectivo para ondas largas [$C(t)/a = \varepsilon(t)$, $L/a = \mu$, y $\beta a << 1$]. Se comprueba experimentalmente comparando los resultados con los teóricos. Los resultados presentados incluyen: la relación de dispersión, generación de armónicos y “golpecitos” en frecuencia.

# Agradecimientos

A Dios Altísimo y a la Madre Santísima por todo lo recibido.

A mi asesor el Dr. Peter Halevi, por su tiempo, paciencia, enseñanzas, dedicación y apoyo.

A mis padres, hermanos e hijo por su apoyo y compañía.

A los Dres. Zurita, Olvera Y Corona por su ayuda y comentarios en diversos aspectos del tema.

Al Dr. Zaldívar por su ayuda con el equipo de laboratorio.

Al INAOE y CONACYT.

A mis amigos y compañeros por su apoyo moral, compañía y discusiones en temas relacionados y no relacionados con este trabajo.

Y al pueblo de México por el ingreso económico recibido en forma de beca.

# Index

# Chapter I

## Introduction

Wave propagation in transmission lines has been the subject of study for many decades. These are constituted by periodically positioned lump components such as capacitors and inductors. Transmission lines can also display temporal periodicity and this paper concerns a low-pass transmission line with both spatial and temporal periodicities. This is achieved by modulating capacitances periodically in time. Our modeling is realistic, taking into account mechanisms of absorption, the non-linearity of the varactors that provide the temporal modulation of the capacitance, and most importantly, the effect that the modulation source has on wave propagation. Spatial periodicity is known to give rise to dispersion relations with frequency gaps and periodicity in the phase advance whereas temporal periodicity results in dispersion relations that are periodic in the frequency and have phase advance gaps. Indeed, our dynamic transmission line (DTL) will be shown, both theoretically and experimentally, to display such phase advance gaps. We also demonstrate that our DTLs possess other characteristics of dynamic media such as harmonic generation and frequency beats. Since the DTL's capacitances are all identically modulated (in tandem) regardless of their location, the capacitance $C(t)$ is a periodic function. This is qualitatively different from the much researched traveling-wave parametric amplifier (TWPA), where $C$ is periodic in the phase $(\beta Na - \Omega t)$ of a traveling pump wave.

DTLs are of great interest, offering spatial and temporal periodicities combined, as well as possibilities of several applications. We expect that all the effects, found for a dynamic medium, can be reproduced in DTLs. In addition, it is expected that DTLs could be used not only as parametric

amplifiers or frequency converters, but also as controllable time delay lines. Transmission velocity is essential in some applications and DTLs might transmit pulse harmonics faster than light. Moreover, a two-dimensional DTL could be used to separate and route composite signals which are omnipresent in modern communications, as well as other applications associated with forbidden bands of the phase advance. Also, the working frequency can range from kHz to THz using split ring resonators.

## 1.1 Objectives

The objectives of this dissertation are:

1) To develop the theory for a realistic dynamic transmission line.

2) To design and fabricate a dynamic transmission line.

3) To prove that there are phase advance gaps for the dispersion of a dynamic transmission line.

4) To prove that there are harmonics of the modulation frequency $\Omega$ when an externally applied signal of frequency $\omega$ is transmitted by a dynamic transmission line.

5) To compare experimental and theoretical results.

## 1.2 Organization of this dissertation

Chapter II of this thesis presents existing theory of TWPAs, as well as previous studies on dielectric media characterized by parameters that vary periodically in time which have a strong connection with this dissertation.

In Chapter III, we present a realistic model for our DTL which includes losses, as well as explicit modulation sources that feed the nonlinear varactors. In continuation, we derive the differential equation for the nodal voltage from Kirchhoff's laws applied to the aforementioned model. Afterward, we present a perturbational solution for the traveling wave and the eigenvalue equation that describes the dispersion relation for our DTL. Next, we show that in the long wavelength limit and neglecting resistance effects, propagation in the DTL can be described by an effective medium.

In Chapter IV, an approximate analytical solution is presented to show that the propagation constant forms two bands $\beta_1(\omega)$ and $\beta_2(\omega)$ that are separated by a band gap. Subsequently, we solve numerically the eigenvalue equation for our realistic model and compare the resulting band structure with that for the approximate analytical solution previously solved. After that, we describe in detail the fabricated DTL, the measurement of the dispersion relation $\beta(\omega)$ and its comparison to theoretical band structures.

Chapter V presents the discussion of some possible applications and the conclusions.

# Chapter II

## Literature on dynamic transmission lines and dynamic media

*In this chapter, a review on traveling wave parametric amplifiers is presented and their qualitatively different modulation procedure is discussed. Additionally, the recent studies of dynamic media that are related with the dynamic transmission line are shown.*

### 2.1 Traveling wave parametric amplifier (TWPA)

A TWPA consists of low-pass filter cells where two voltage signals are launched: a traveling wave signal to be amplified and a pumping wave signal that modulates the capacitances of the TWPA. The pumping wave is applied at the input or output end of the TWPA and each capacitance varies with the phase of the traveling pumping wave. In the 1960s, TWPAs were widely studied after Cullen showed that parametric excitation of an electric oscillatory circuit was possible, and that any method of periodically varying the capacitance or the inductance could be used [1]. A year later, Cullen extended his work by incorporating the effect of attenuation due to resistance losses and the effect of saturation at large signal levels [2]. Almost at the same time, Tien and Suhl proposed a TWPA which consisted of two transmission lines embedded in a ferromagnetic medium. The medium was energized by a traveling wave, providing a time- and distance-dependent coupling between the lines [3]. Months later, Tien investigated the effects of positive or negative phase and group velocities, and determined that amplification is possible only when the traveling and the pumping wave have group velocities of different signs [4]. Ashkin et al. used an electron beam to

modulate the shunt capacitors [5]. An analysis demonstrated that in systems with “little” dispersion, the pumping will not result in amplification but rather in energy conversion to multiple harmonics of the pumping frequency, such that TWPAs might be used as frequency converters [6]. Studies of the pump wave´s phase velocity effect were realized, and Brillouin diagrams showed that there are frequency stop bands and periodicity as function of the phase advance $\beta a$ when the TWPA is used as an amplifier [7].

In ref. [8] a TWPA with eight diodes in a waveguide was fabricated and investigated, focusing only on amplification; the diodes were modulated by the phase of the pump wave. However, the TWPA impedance could not be matched at the ends due to its time-changing nature and a high gain could not been obtained. Also, a TWPA based on coupled cavities was proposed and fabricated [9]. Cassedy widely studied the dispersion relations of TWPAs; he concluded that when the capacitance is modulated in time in a traveling wave fashion, the phase advance has complex values, even for a lossless low-pass transmission line [11]. Later he found, that there are forbidden bands for the real part of the phase advance $\beta a$, and that its imaginary part is not zero at this gap [12]. He also extended this work to consider the effects of all the harmonics [13] and studied wave propagation under the influence of temporal and spatial periodicity, focusing on the dominant harmonics $n = 0$ and $n = -1$ [14].

Noise greatly affected the performance of TWPAs; active networks were investigated in order to improve their bandwidth and flat gain response [15], as well as the effect that TWPAs’ resistance value had on amplification [16]. Also, a microstrip parametric amplifier with a hyperabrupt varactor was made, improving the gain, bandwidth, and noise level of the amplifier [17]. The use of tunnel diodes as a replacement for varactors, with the aim of reducing circuit speed, was also considered [18]. Regarding frequency conversion, measurement of the spectral performance showed that TTL logic digital

dividers had a better performance than parametric dividers using varactors with a low quality factor [19]. Nevertheless, high quality factor varactors have low power consumption and are highly tunable; for these reasons their manufacture improved UHF applications [20] and they can be used to parametrically amplify large signals [21]. Recently, a dynamic low-pass filter using varactors in a CMOS process has been simulated to be used as a frequency divider and as a parametric amplifier [22]. Last year, a time-varying transmission-line with varactor diodes was implemented and proposed as a circulator device that allows transmission and reception of signals at the same time and the same frequency [24].

## 2.2 Dynamic media

A former study [25] was based on a hypothetic lossless DTL with time-periodic shunt capacitances, however without specifying the source of modulation. As a result, the nodal voltage itself was identified as the traveling signal wave. A DTL can be represented as an effective medium if electromagnetic waves propagating in this medium and in the DTL obey the same dispersion relation $\omega(\beta)$. This occurs in the long wavelength limit $\beta a << 1$, where the distributed capacitance and inductance can be described in terms of an effective permittivity and permeability, respectively. Previously, it was found that the dispersion relation for such a dynamic medium with periodic permittivity $\varepsilon(t)$ is periodic in $\omega$ and that there are forbidden bands for the phase advance $\beta$ [26]. Also, when a monochromatic plane wave of frequency $\omega$ is incident on such a medium, the reflected and transmitted waves contain harmonics of the modulation frequency $\Omega$ [26]. Later, it was reported that a dynamic slab exhibits parametric resonances for odd multiples of one-half of the modulation frequency $\omega = (\Omega/2)(2l+1)$, provided that the

slab thickness assumes certain particular values [27]. Furthermore, when a quasi-monochromatic pulse of carrier frequency $\omega_C$ is incident at a dynamic slab, it generates quasi-monochromatic pulses of the harmonics $|\omega_C - n\Omega|$ and, in some cases, the peaks of these harmonics can emerge on the other side of the slab faster than light in vacuum [28].

# Chapter III

## Modeling, general solution and effective medium for the dynamic transmission line

*In this chapter, at first, a realistic model for the dynamic transmission line is introduced. Subsequently, the derivation of the differential equation for the nodal voltage considering the traveling wave and the modulation wave is shown. In addition, the perturbational solution for the traveling wave and the resulting eigenvalue equation are given. Finally, the effective medium description is presented.*

### 3.1. Realistic modeling of the externally modulated transmission line

A ***dynamic transmission line*** (**DTL**) can be implemented using microstrip technology. A microstrip consists of a dielectric substrate with a ground level copper layer at the bottom and a copper line at the top. The microstrip has a capacitance and an inductance per unit length and their values can be modified inserting lumped elements. The modulation in time can be achieved by means of varactors, which are solid state devices whose capacitance can be regulated by a dc voltage. However, such a capacitance can become time-dependent, if the voltage governing it has an ac component. Indeed, the capacitances of our DTL are controlled by an ac voltage and a dc voltage for inverse polarization. In the present study, the voltage applied to the varactors is harmonic, namely $V_\Omega(t) = \overline{V}_\Omega[1 + m\sin(\Omega t)]$. Here $\overline{V}_\Omega$ is the inverse polarization voltage and $\Omega/2\pi$ and $m$ are, respectively, the modulation frequency and strength (or, briefly, “modulation”) of the ac voltage.

A realistic description of the DTL requires considering not only the modulation voltage $V_\Omega(t)$, but also a finite conductivity for the microstrip copper line, modeled as a series resistance $R$; substrate losses modeled as a shunt conductance $G$; a current leakage through the modulation feeding lines corresponding to the resistance $R_\Omega$; and a parasitic capacitance $C_P$ associated with the microstrip (that cannot be modulated). The resistance $R_\Omega$ has to be chosen very high, so as to avoid current flow through the voltage source (that would diminish the modulation intensity $m$) [see Appendix A]. The unit cell of the DTL is shown in Fig. 3.1 along with the currents and voltages at the nodes $N$ and $N$+1.

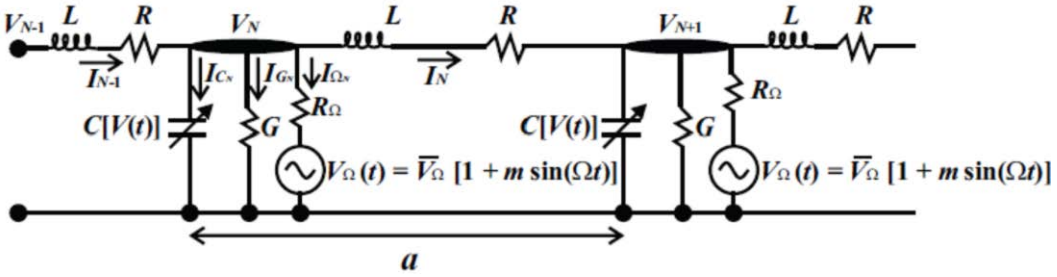


Figure 3.1. Low-pass DTL unit-cell of length *a* between nodes $N$ and $N + 1$. The voltages $V_\Omega(t)$ have the same amplitude and phase at all nodes. As a result, the capacitances $C[V(t)]$ are modulated in tandem, and the voltage difference $V_N - V_{N+1}$ is given by only the (small) signal voltage of frequency $\omega$ of the traveling wave.

If the capacitance is voltage dependent, then the ac current through such a capacitor is

$$I(t) = \frac{dQ}{dt} = \frac{d}{dt}\left[C(V)V(t)\right]. \tag{3.1}$$

It follows that

$$I(t) = \left\{C\left[V(t)\right] + \frac{dC}{dV}V(t)\right\}\frac{dV}{dt}. \tag{3.2}$$

Thus we see that, because of the dependence of $C$ on $V$, the current is not determined by the capacitance itself, but rather by the expression in the curly brackets, which we name as *dynamic capacitance*, being of interest only if the current and voltage are time-dependent. Other expressions, such as incremental capacitance, differential capacitance, and junction capacitance are also used.

For convenience, we include the parasitic capacitance $C_P$ in our definition of the dynamic capacitance:

$$\tilde{C}(V)=C(V)+\frac{dC}{dV}V+C_P. \tag{3.3}$$

Then the current through a varactor in Fig. 2 is, simply,

$$I_C(t)=\tilde{C}[V(t)]\frac{dV}{dt}. \tag{3.4}$$

The dependences of the dynamic and conventional capacitances on applied voltage are shown in Fig. 3.2.

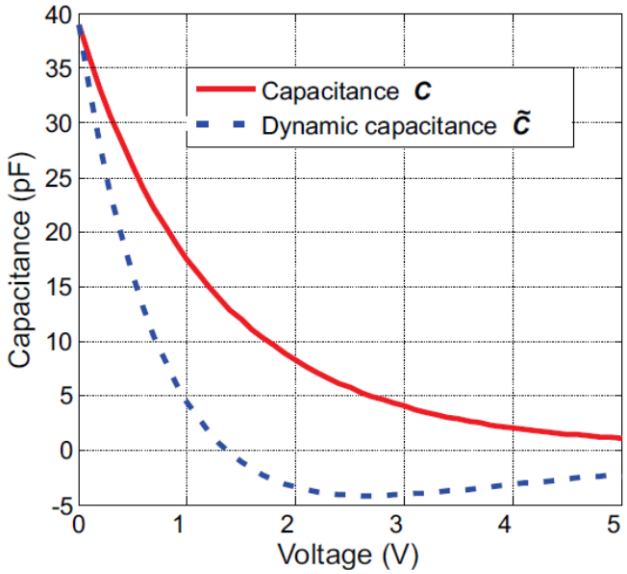


Figure 3.2. Low-pass Conventional and dynamic capacitances as function of applied voltage for the varactor diodes in the DTL.

It is significant that, unlike the conventional capacitance $C(V)$, the dynamic capacitance can be negative for a range of voltages, as seen in the figure.

## 3.2 Derivation of differential equation for the nodal voltage

Applying Kirchhoff's current law to node $N$ in Fig. 3.1, we have

$$I_{N-1} - I_N = I_{C_N} + I_{G_N} + I_{\Omega_N} . \tag{3.5}$$

Next, we apply the operator $Ld/dt$ to the last equation:

$$L\frac{d\left(I_{N-1}\right)}{dt} - L\frac{d\left(I_N\right)}{dt} = L\frac{d\left(I_{C_N}\right)}{dt} + L\frac{d\left(I_{G_N}\right)}{dt} + L\frac{d\left(I_{\Omega_N}\right)}{dt} . \tag{3.6}$$

Using Kirchhoff's voltage law, the voltage difference between nodes can be expressed in terms of the resistance $R$, the inductance $L$, and the corresponding currents as

$$V_{N-1} - V_N = L\frac{d\left(I_{N-1}\right)}{dt} + RI_{N-1} , \tag{3.7a}$$

$$V_N - V_{N+1} = L\frac{d\left(I_N\right)}{dt} + RI_N . \tag{3.7b}$$

The currents associated with the resistance $R_\Omega$ and the conductance $G$ on node $N$ are given by

$$I_{\Omega_N} = \left(V_N - V_\Omega\right)/R_\Omega \tag{3.8a}$$

and

$$I_{G_N} = GV_N \,. \qquad (3.8b)$$

According to eq. (3.4), the current through the varactor is $I_{C_N} = \tilde{C}(V_N)\,dV_N/dt$ .

With the help of eqs. (3.7), (3.8), (3.5), and with the abbreviation $G_R = G + 1/R_\Omega$, eq. (3.6) can be rewritten as

$$V_{N-1} + V_{N+1} - 2V_N - R\tilde{C}(V_N)\frac{dV_N}{dt} - RG_R V_N - L\frac{d}{dt}\left[\tilde{C}(V_N)\frac{dV_N}{dt}\right] - LG_R\frac{dV_N}{dt} = -\frac{R}{R_\Omega}V_{\Omega_S} - \frac{L}{R_\Omega}\frac{dV_{\Omega_S}}{dt}. \qquad (3.9)$$

In the next section we will proceed to solve this equation for the signal voltage wave.

## 3.3. Perturbational solution for the signal wave and the eigenvalue equation

In Appendix I we show that, to a good approximation, the nodal voltage $V_N(t)$ is composed of the modulation voltage $V_\Omega(t)$ and the wave signal $v_N(t)$:

$$V_N(t) = V_\Omega(t) + v_N(t)\,. \qquad (3.10)$$

We also assume that the latter voltage is much smaller than the former,

$$|v_N(t)| << |V_\Omega(t)|\,, \qquad (3.11)$$

so that the varactor modulation is mostly due to the modulation voltage $V_\Omega(t)$. The capacitance as a function of nodal voltage can be then written approximately as

$$\tilde{C}(V_N) = \tilde{C}(V_\Omega) + \tilde{C}'(V_\Omega)\,v_N(t)\,, \qquad (3.12)$$

where the prime implies differentiation with respect to the argument. The small signal voltage on node $N$ can be expressed as $v_N(t) = v(t)e^{j\beta aN}$. It follows that

$$v_{N\pm1}(t) = v_N(t)e^{\pm j\beta a}. \tag{3.13}$$

The eqs. (3.10) and (3.13) imply that the first three terms of eq. (3.9) are proportional to $v_N(t)$:

$$V_{N-1} + V_{N+1} - 2V_N = v_{N-1} + v_{N+1} - 2v_N = \left(e^{-j\beta a} + e^{j\beta a} - 2\right)v_N = 2(\cos\beta a - 1)v_N.$$

Then eq. (3.9) can be written as

$$\begin{aligned} &-4\sin^2(\beta a/2)v_N(t) - R\left[\tilde{C}(V_\Omega) + \tilde{C}'(V_\Omega)v_N(t)\right]\left[\dot{V}_\Omega(t) + \dot{v}_N(t)\right] \\ &\quad - RG_R\left[V_\Omega(t) + v_N(t)\right] - LG_R\left[\dot{V}_\Omega(t) + \dot{v}_N(t)\right] \\ &\quad - L\frac{d}{dt}\left\{\left[\tilde{C}(V_\Omega) + \tilde{C}'(V_\Omega)v_N(t)\right]\left[\dot{V}_\Omega(t) + \dot{v}_N(t)\right]\right\} \\ &\quad = -\frac{R}{R_\Omega}V_\Omega(t) - \frac{L}{R_\Omega}\dot{V}_\Omega(t), \end{aligned} \tag{3.14}$$

where ($\cdot$) means derivative with respect to time.

Now, we group together the terms proportional to $v_N(t)$, $\dot{v}_N(t)$, and $\ddot{v}_N(t)$ (neglecting the quadratic expressions) resulting in the following inhomogeneous differential equation:

$$\begin{aligned} &\left[4\sin^2(\beta a/2) + R\tilde{C}'(V_\Omega)\dot{V}_\Omega(t) + RG_R + L\tilde{C}''(V_\Omega)\dot{V}_\Omega^2(t) + L\tilde{C}'(V_\Omega)\ddot{V}_\Omega(t)\right]v_N(t) \\ &\quad + \left[R\tilde{C}(V_\Omega) + 2L\tilde{C}'(V_\Omega)\dot{V}_\Omega(t) + LG_R\right]\dot{v}_N(t) + \left[L\tilde{C}(V_\Omega)\right]\ddot{v}_N(t) \\ &\quad = -L\tilde{C}(V_\Omega)\ddot{V}_\Omega(t) - \left[L\tilde{C}'(V_\Omega)\dot{V}_\Omega(t) + R\tilde{C}(V_\Omega) + LG\right]\dot{V}_\Omega(t) - RGV_\Omega(t). \end{aligned} \tag{3.15}$$

Equation (3.15) has the form ($N$ being arbitrary)

$$S(t)\frac{d^2v(t)}{dt^2}+T(t)\frac{dv(t)}{dt}+U(t)v(t)=F(t)\,, \tag{3.16}$$

where

$$S(t)=L\tilde{C}\left(V_\Omega\right), \tag{3.17a}$$

$$T(t)=2L\tilde{C}'\left(V_\Omega\right)\dot{V}_\Omega(t)+R\tilde{C}\left(V_\Omega\right)+LG_R\,, \tag{3.17b}$$

$$\begin{aligned}U(t)=&\,4\sin^2\left(\beta a/2\right)+L\tilde{C}'\left(V_\Omega\right)\ddot{V}_\Omega(t)+L\tilde{C}''\left(V_\Omega\right)\dot{V}_\Omega{}^2(t)\\&+RG_R+R\tilde{C}'\left(V_\Omega\right)\dot{V}_\Omega(t)\end{aligned}\,, \tag{3.17c}$$

$$\begin{aligned}F(t)=&-L\tilde{C}\left(V_\Omega\right)\ddot{V}_\Omega(t)-\left[L\tilde{C}'\left(V_\Omega\right)\dot{V}_\Omega(t)+R\tilde{C}\left(V_\Omega\right)+LG\right]\dot{V}_\Omega(t)\\&-RGV_\Omega(t).\end{aligned} \tag{3.17d}$$

The solution of this linear inhomogeneous equation is given by the sum of a particular solution of the inhomogeneous equation and two independent solutions of the homogeneous equation. Note that the functions, $S(t)$, $T(t)$, $U(t)$, and $F(t)$ are all periodic in time, having the period $2\pi/\Omega$. Then we assume that the particular solution of the inhomogeneous equation, denoted as $v_F(t)$ is also periodic in time with the same period $2\pi/\Omega$:

$$v_F(t)=\sum_n v_F e^{jn\Omega t}\,. \tag{3.18}$$

Substitution in the inhomogeneous differential equation gives

$$\begin{aligned}&\sum_m S_m e^{jm\Omega t}\sum_n v_n(jn\Omega)^2 e^{jn\Omega t}+\sum_m T_m e^{jm\Omega t}\sum_n v_n(jn\Omega)e^{jn\Omega t}\\&\quad+\sum_m U_m e^{jm\Omega t}\sum_n v_n e^{jn\Omega t}=\sum_n F_n e^{jn\Omega t}.\end{aligned} \tag{3.19}$$

It follows that

$$\sum_m \left\{ \sum_n \left[ S_{m-n}(jn\Omega)^2 + T_{m-n}(jn\Omega) + U_{m-n} \right] v_n - F_n \delta_{mn} \right\} e^{jm\Omega t} = 0 . \qquad (3.20)$$

This will be satisfied for any instant of time $t$ if

$$\sum_n \left[ U_{m-n} + jn\Omega T_{m-n} - n^2\Omega^2 S_{m-n} \right] v_n = F_m . \qquad (3.21)$$

This is a set of linear inhomogeneous equations that can be readily solved for the $v_n$. However, our interest in this thesis lying in propagating normal modes (rather than forced modes solutions), we will not pursue this direction.

We turn then to the homogeneous differential equation. One solution has the form of a temporal Bloch wave, namely a harmonic oscillation $e^{-j\omega t}$ with a periodically modulated amplitude $\sum_n \tilde{v}_n e^{jn\Omega t}$ :

$$\tilde{v}(t) = \sum_n \tilde{v}_n e^{j(n\Omega-\omega)t} . \qquad (3.22)$$

Substitution in eq. (3.16) with $F(t) = 0$ gives

$$\begin{aligned} \sum_m S_m e^{jm\Omega t} \sum_n \tilde{v}_n (in\Omega - i\omega)^2 e^{j(n\Omega-\omega)t} + \sum_m T_m e^{jm\Omega t} \sum_n \tilde{v}_n (jn\Omega - j\omega) e^{j(n\Omega-\omega)t} \\ + \sum_m U_m e^{jm\Omega t} \sum_n \tilde{v}_n e^{j(n\Omega-\omega)t} = 0. \end{aligned} \qquad (3.23)$$

It follows that

$$\sum_m \sum_n \left[ U_m + T_m(jn\Omega - j\omega) + S_m(jn\Omega - j\omega)^2 \right] \tilde{v}_n e^{j(m+n)\Omega t} = 0 . \qquad (3.24)$$

This will be satisfied at all times provided that

$$\sum_n \left[ U_{m-n} + j(n\Omega - \omega) T_{m-n} - (n\Omega - \omega)^2 S_{m-n} \right] \tilde{v}_n = 0 . \qquad (3.25)$$

Because $U_{m-n}$ depends on $\beta$, this is an eigenvalue equation that determines the dispersion relation $\omega(\beta)$.

## 3.4. Effective medium description

In this section we show that for waves of long wavelength $2\pi/\beta$ in comparison with the period $a$, propagation in the DTL can be described by an effective medium approximation. Thus $\beta a << 1$ and the first term in eq. (3.17c) may be approximated as $\beta^2 a^2$. We also neglect all mechanisms of absorption ($R = 0$, $G = 0$, $R_\Omega = \infty$) and "switch off" the direct effects of modulation [$F(t) = 0$]. Then eq. (3.15) simplifies as

$$L\tilde{C}(V_\Omega)\frac{d^2v}{dt^2} + 2L\tilde{C}'(V_\Omega)\dot{V}_\Omega(t)\frac{dv}{dt} + \left[\beta^2 a^2 + L\tilde{C}'(V_\Omega)\ddot{V}_\Omega(t) + L\tilde{C}''(V_\Omega)\dot{V}_\Omega^2(t)\right]v(t) = 0. \tag{3.26}$$

This can be rewritten as

$$\frac{L}{a}\frac{\tilde{C}(V_\Omega)}{a}\frac{d^2v}{dt^2} + 2\frac{L}{a}\frac{d}{dt}\left[\frac{\tilde{C}(V_\Omega)}{a}\right]\frac{dv}{dt} + \left\{\beta^2 + \frac{L}{a}\frac{d^2}{dt^2}\left[\frac{\tilde{C}(V_\Omega)}{a}\right]\right\}v(t) = 0\,, \tag{3.27}$$

or, compactly, as

$$\frac{L}{a}\frac{d^2}{dt^2}\left\{\frac{\tilde{C}(V_\Omega)}{a}v(t)\right\} + \beta^2 v(t) = 0\,. \tag{3.28}$$

Compare eq. (3.28) with the wave equation for a plane wave propagating in a dielectric medium of dynamic permittivity $\varepsilon(t)$ and permeability $\mu$ (= const). It has been derived in ref. [26], although with the assumption that $\mu = \mu_0$ (the vacuum permeability). The generalization to $\mu \neq \mu_0$ is straightforward and reads

$$\mu\frac{d^2}{dt^2}\{\varepsilon(t)E(t)\} + \beta^2 E(t) = 0\,. \tag{3.29}$$

From the comparison we then conclude that the properties of a voltage wave propagating in a DTL are identical to the properties of an electromagnetic wave that propagates in a dielectric ("effective") medium provided that

$\tilde{C}\left[V_{\Omega}(t)\right]/a = \varepsilon(t)$ for all $t$, (3.30a)

$L/a = \mu$, (3.30b)

$\beta a << 1$, (3.30c)

losses are negligible. (3.30d)

We note that in this section no particular model has been assumed for the varactor, that is, the function $\tilde{C}(V_{\Omega})$ is arbitrary. Moreover, neither has the form of the temporal modulation been restricted; thus $V_{\Omega}(t)$ is not necessarily a periodic function, as far as eq. (3.30a) is concerned.

# Chapter IV

## Theoretical and experimental results

*In this chapter an approximate solution based on a linear model of the varactor and weak modulation is presented. Numerical solutions for the electromagnetic band structure for different values of the most important parameters are shown. Experimental procedure, comparison between theoretical and experimental results, and experimental results are explained in detail*

### 4.1 Linear modeling of varactor and the approximation of weak modulation

Rather than turning to a numerical solution of the eigenvalue equation (3.25) we will first solve it analytically, subject to appropriate approximations. Our purpose is to show that two bands are obtained for the propagation constant, $\beta_1(\omega)$ and $\beta_2(\omega)$, and that these bands are separated by a band gap that is proportional to the modulation $m$. A linear approximation for the dynamic capacitance suffices if $m$ << 1:

$$\tilde{C}(V) = \tilde{C}(\overline{V}) + \frac{d\tilde{C}}{d\overline{V}}(V - \overline{V}) . \qquad (4.1)$$

We also assume harmonic modulation,

$$V_\Omega(t) = \overline{V}_\Omega \left(1 + m \sin \Omega t\right) . \qquad (4.2)$$

With the abbreviations, $\tilde{C}(\overline{V}) = \tilde{C}$ and $d\tilde{C}/d\,\overline{V} = \tilde{C}'$, eq. (4.1) becomes

$$\tilde{C}(\overline{V}, t) = \tilde{C} + \tilde{C}' \overline{V} m \sin \Omega t , \qquad (4.3)$$

or,

$$\tilde{C}(\overline{V},t)=\tilde{C}(1+M\sin\Omega t)\,,\qquad M=\tilde{C}'\overline{V}m/\tilde{C}\,. \tag{4.4}$$

Then the only nonvanishing Fourier components in eq. (3.17) are

$$S_0=L\tilde{C}\,, \tag{4.5a}$$

$$S_{\pm1}=\mp(i/2)ML\tilde{C}\,, \tag{4.5b}$$

$$T_0=LG_R+R\tilde{C}\,, \tag{4.5c}$$

$$T_{\pm1}=M\tilde{C}\left(\Omega L\mp iR/2\right), \tag{4.5d}$$

$$U_0=4\sin^2(\beta a/2)+RG_R\,, \tag{4.5e}$$

$$U_{\pm1}=M\tilde{C}\Omega\left(R\pm i\Omega L\right)/2\,. \tag{4.5f}$$

From eq. (4.4) we see that the modulation $M$ of the dynamic capacitance $\tilde{C}(t)$ can be quite different than the modulation $m$ of the voltage $V_\Omega(t)$. In the case of weak modulation, the important harmonics are $n$ = 0 and $n$ = 1. This follows form the *empty lattice model* of periodicity [29] applied to temporal modulation of the capacitance. We will then restrict the values of $m$ and $n$ in eq. (3.25) to 0 or 1. This results in the two homogeneous equations

$$\begin{aligned}\left(U_0-i\omega T_0-\omega^2S_0\right)\tilde{v}_0+\left[U_{-1}+i(\Omega-\omega)T_{-1}-(\Omega-\omega)^2S_{-1}\right]\tilde{v}_1&=0,\\ \left(U_1-i\omega T_1-\omega^2S_1\right)\tilde{v}_0+\left[U_0+i(\Omega-\omega)T_0-(\Omega-\omega)^2S_0\right]\tilde{v}_1&=0.\end{aligned} \tag{4.6}$$

The determinant of the coefficients of $\tilde{v}_0$ and $\tilde{v}_1$ must vanish, hence

$$\begin{aligned}&\left(U_0-i\omega T_0-\omega^2S_0\right)\left(U_0+i(\Omega-\omega)T_0-(\Omega-\omega)^2S_0\right)\\ &\quad-\left(U_1-i\omega T_1-\omega^2S_1\right)\left(U_{-1}+i(\Omega-\omega)T_{-1}-(\Omega-\omega)^2S_{-1}\right)=0.\end{aligned} \tag{4.7}$$

It is easy to see that this leads to a quadratic equation for $\sin^2(\beta a/2)$ and, therefore, two bands $\beta_1(\omega)$ and $\beta_2(\omega)$. These are plotted in sec. 4.2 and are compared with the "exact" band structure. The closest approach between these bands occurs at the frequency $\omega = \Omega/2$, to which we restrict the calculation that follows. Substitution of the eqs. (4.5) in eq. (4.7) leads to the approximate result

$$4\sin^2(\beta a/2) = \tilde{\Omega}^2/4 - RG_R \pm (\tilde{\Omega}^2/8)\left[M^2 - 16\left(G_R/\Omega\tilde{C} + R/\Omega L\right)^2\right]^{1/2}. \quad (4.8)$$

Here we defined the normalized circular frequency ($\tilde{C}$ > 0) as:

$$\tilde{\Omega} = \Omega\sqrt{L\tilde{C}}\,. \quad (4.9)$$

First we analyze the lossless case, with $R$ = $G$ = 0 and $R_\Omega \rightarrow \infty$. Then we can express eq. (4.8) compactly as

$$2\sin(\beta_\pm a/2) = (\tilde{\Omega}/2)(1 \pm M/2)^{1/2}. \quad (4.10)$$

This equation has two solutions for $\beta$, provided that $(\tilde{\Omega}/4)(1+M/2)^{1/2} \le 1$. Therefore, having assumed weak modulation ($M$ << 1) in this section, the parameter $\tilde{\Omega}$ cannot be greater than 4. Namely, if $\tilde{\Omega}$ > 4, no propagation can take place in the DTL for frequencies $\omega \simeq \Omega/2$. This establishes the important characteristic of a periodically modulated DTL, that there are two bands, $\beta_-(\omega)$ or $\beta_1(\omega)$ and $\beta_+(\omega)$ or $\beta_2(\omega)$, separated by a *β-gap* whose width is proportional to the modulation.

If $\sin(\beta a/2)$ << 1, namely, in the long wavelength limit $\beta a << 1$, eq. (4.10) becomes

$$\beta_{\pm} a \simeq \left(\tilde{\Omega}/2\right)\left(1 \pm M/2\right)^{1/2}, \tag{4.11}$$

and with $\beta_{\pm} \simeq \overline{\beta} \pm \Delta\beta/2$, the forbidden band gap is

$$\Delta\beta a \simeq \tilde{\Omega} M/4, \quad M << 1 \tag{4.12}$$

or

$$\Delta\beta/\overline{\beta} \simeq M/2. \tag{4.13}$$

Thus, in this approximation, the normalized gap only depends on the modulation of the capacitors.

Returning to consider the resistances $R$, $1/G$, and $R_{\Omega}$, eq. (4.8) can be rewritten as

$$4\sin^2\left(\beta a/2\right) = \left(\tilde{\Omega}^2/4\right) - RG_R \pm \left(\tilde{\Omega}^2/8\right)\left[M^2 - M_R^2\right]^{1/2}. \tag{4.14}$$

where

$$M_R = 4\left(G_R/\Omega\tilde{C} + R/\Omega L\right). \tag{4.15}$$

According to eq. (4.14), there are three possible behaviors for the phase advances $\beta a$:

1) $M > M_R$. The square root is real, so that the phase advances are real, $\beta_+ \neq \beta_-$, and there is a band gap $\Delta\beta = \beta_+ - \beta_-$. In the approximation considered, two undamped waves propagate.

2) $M = M_R$. Now $\beta_+ = \beta_- = \overline{\beta}$, and the solution reduces to

$$2\sin\left(\beta a/2\right) \simeq (\tilde{\Omega}/2)\left(1 - 2RG_R/\tilde{\Omega}^2\right). \tag{4.16}$$

Hence, the two $\beta$-bands now touch at $\omega = \Omega/2$ and there is no $\beta$-gap. Only a single wave propagates.

3) $M < M_R$. The square root is imaginary, so approximately

$$4\sin^2\left(\beta a/2\right) \cong \left(\tilde{\Omega}^2/4\right) \pm j\left(\tilde{\Omega}^2/8\right)\left(M_R^2 - M^2\right)^{1/2}. \qquad (4.17)$$

This has solutions of the form $\beta = \beta'\left(1 \pm j\kappa\right)$, where $\beta'$ and $\kappa$ are real and $\kappa << \beta'$ (= $\mathrm{Re}\beta$). If $\beta a << 1$, and considering that the first term on the right side is much greater than the second term we have

$$\beta a \simeq (\tilde{\Omega}/2)\left[1 + (j/4)\left(M_R^2 - M^2\right)^{1/2}\right]. \qquad (4.18)$$

Here, we have selected the physically correct sign of the square root (+) that gives rise to attenuation. A single damped wave propagates.

## 4.2. Numerical results for the electromagnetic band structure

In the previous section a linear model was considered for the dynamic capacitance of the varactors. Now we proceed to a very accurate modeling and present the resulting dispersion curves. The dynamic capacitance is described by the quadratic expansion

$$\tilde{C}(V) = \tilde{C} + \tilde{C}'(V - \bar{V}) + \frac{1}{2}\tilde{C}''(V - \bar{V})^2. \qquad (4.19)$$

With harmonic modulation, eq. (4.2), this becomes

$$\tilde{C}(V) = \tilde{C} + \tilde{C}M\sin\Omega t + \tilde{C}''\bar{V}_\Omega{}^2 m^2 \sin^2(\Omega t)/2, \qquad (4.20)$$

where the capacitance modulation $M$ has been defined in eq. (4.4) and its relation with $m$ is shown in Fig. 4.1 .

The only nonvanishing Fourier components of eqs. (3.17a-c) are

$$S_0 = L\left(\tilde{C} + Q\right), \qquad (4.21a)$$

$$S_{\pm 1} = \mp jL\tilde{C}M/2, \tag{4.21b}$$

$$S_{\pm 2} = -LQ/2, \tag{4.21c}$$

$$T_0 = LG_R + R\left(\tilde{C} + Q\right), \tag{4.21d}$$

$$T_{\pm 1} = \tilde{C}M\left(\Omega L \mp jR/2\right), \tag{4.21e}$$

$$T_{\pm 2} = -Q\left(R/2 \pm j2\Omega L\right), \tag{4.21f}$$

$$U_0 = 4\sin^2\left(\beta a/2\right) + RG_R, \tag{4.21g}$$

$$U_{\pm 1} = \Omega\tilde{C}M\left(R \pm j\Omega L\right)/2, \tag{4.21h}$$

$$U_{\pm 2} = \Omega Q\left(2\Omega L \mp jR\right), \tag{4.21i}$$

where

$$Q = \tilde{C}''\bar{V}_\Omega{}^2 m^2/4, \qquad \tilde{C}'' = d^2\tilde{C}(V)/d\bar{V}^2\,. \tag{4.22}$$

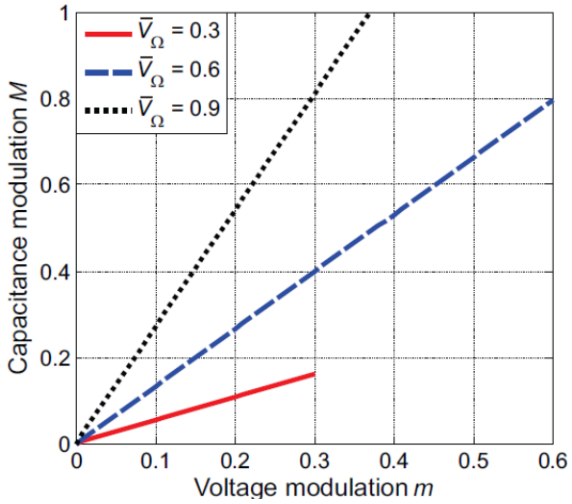


Figure. 4.1. Capacitance modulation $M$ versus voltage modulation $m$, according to eq. (6.4) for three values of the polarization voltage $\bar{V}_\Omega$ in volts. Voltage modulation $m$ for $\bar{V}_\Omega$ = 0.3 volts cannot be greater than 0.3 to avoid direct polarization of the varactor, where the varactor stops behaving as a voltage dependent capacitor.

Using eqs. (4.21), we solved numerically eq. (3.25) and compared the results with the ones obtained by the approximate dispersion relation given by eq. (4.7). Fig. 4.2 shows the dispersion curves for the accurate and the approximate solutions for two different values of modulation. For all subsequent figures the inductance value is $L$ = 11.85 nH. As expected, the forbidden band gap is directly associated with the modulation intensity $m$.

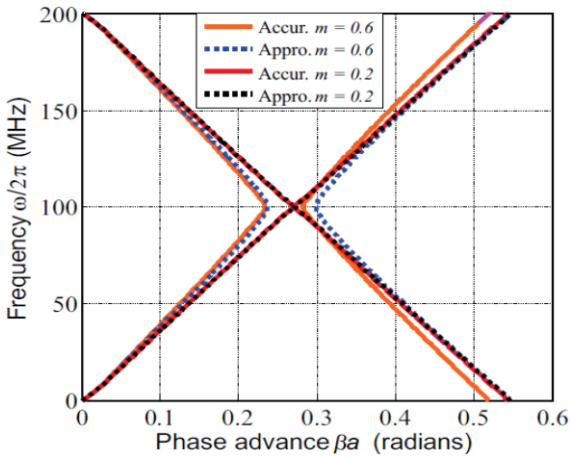


Figure 4.2. Accurate and approximate dispersion relations for two values of the voltage modulation strength $m$. The solutions have an excellent agreement for the weak modulation ($m$ = 0.2), but the approximate band structure is not as accurate for the second $\beta$ band for $m$ = 0.6. The parameter values are $R_\Omega$ = 800 ohms, $G$ = 0.001 mhos, $R$ = 0.24 ohms, $\bar{V}_\Omega$ = 0.6 volts, and $\Omega/2\pi$ = 200 MHz.

Figure 4.3 shows the dispersion relations as function of the polarization voltage $\bar{V}_\Omega$. The approximate solution describes extremely well the DTL dispersion relation, failing only for the second band in case of $\bar{V}_\Omega$ = 0.9 volts. Because this solution is not limited to small values of the phase advance $\beta a$, it can mimic well the accurate solution even for $\beta a \gtrsim 1$. In fig. 4.3 the voltage modulation has the same value $m$ = 0.3, but the capacitance modulation values are different for each value of $\bar{V}_\Omega$: $M$ = 0.16 for $\bar{V}_\Omega$ = 0.3, $M$ = 0.39 for $\bar{V}_\Omega$ = 0.6, and $M$ = 0.81 for $\bar{V}_\Omega$ = 0.9. As a consequence, there is not even a

band gap for $\bar{V}_\Omega$ = 0.3 even though the associated phase advance is greater due to a larger capacitance, but there is a band gap for $\bar{V}_\Omega$ = 0.9 while the corresponding $\beta a$ values are the smallest.

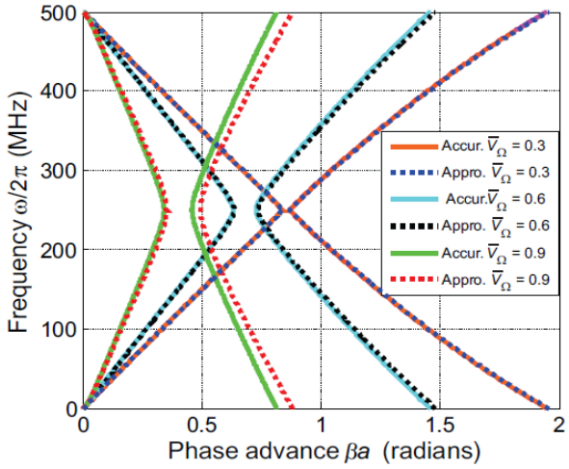


Figure 4.3. Accurate and approximate dispersion relations for three values of the polarization voltage $\bar{V}_\Omega$. The modulation intensity and resistances are the same for all curves. Capacitance values depend on $\bar{V}_\Omega$ and, as a consequence, they are different for each voltage value. The parameters are $R_\Omega$ = 800 ohms, $G$ = 0.001 mhos, $R$ = 0.24 ohms, $m$ = 0.3, and $\Omega/2\pi$ = 500 MHz.

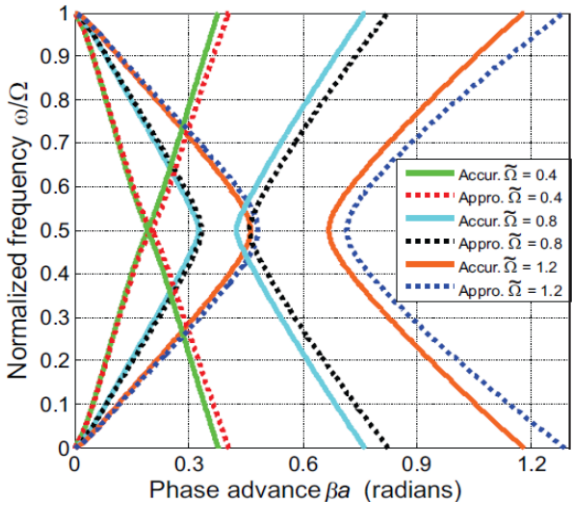


Figure 4.4. Accurate and approximate dispersion relations for three values of the normalized modulation frequency $\tilde{\Omega}$. All the other parameters of the DTL are identical: $R_\Omega$ = 800 ohms, $G$ = 0.001 mhos, $R$ = 0.34 ohms, $m$ = 0.3, and $\bar{V}_\Omega$ = 0.9 volts.

Fig. 4.4 presents the dispersion relations for different values of the normalized modulation frequency $\tilde{\Omega}\,(=\Omega\sqrt{L\tilde{C}}\,)$. The dispersion curves are qualitatively different than those in Fig. 4.3. In Fig. 4.3 the wider band gap occurs at small values of the phase advance, whilst in Fig. 4.4 this happens for the larger values of $\beta a$. In fig. 4.4 three different values of $\tilde{\Omega}$ are considered. For higher values of $\tilde{\Omega}$ (and of the modulation frequency $\Omega$) the capacitance modulation $M$ needed to overcome losses, in order to have a band gap, decreases as follows from eq. (4.15).

Table 4.1. Comparison of accurate solutions [of eq. (3.25)] and approximate solutions [of eq. (4.8)] for the DTL. Here $R_\Omega$ = 2000 ohms, $G$ = 0.001 mhos, $R$ = 0.12 ohms, and $\bar{V}_\Omega$ = 0.6 volts.

| | $\bar{\beta}a$ | | $\Delta\beta a$ | | $\Delta\beta/\bar{\beta}$ | |
|---|---|---|---|---|---|---|
| | Approx. | Accurate | Approx. | Accurate | Approx. | Accurate |
| $\tilde{\Omega}$ = 0.4, $M$ = 0.4 | 0.2002 | 0.1978 | 0.0 | 0.0 | 0.0 | 0.0 |
| $\tilde{\Omega}$ = 0.4, $M$ = 0.5 | 0.1996 | 0.1958 | 0.0204 | 0.0119 | 0.1022 | 0.0608 |
| $\tilde{\Omega}$ = 0.4, $M$ = 0.6 | 0.1991 | 0.1934 | 0.0396 | 0.0325 | 0.1989 | 0.1680 |
| $\tilde{\Omega}$ = 0.6, $M$ = 0.4 | 0.3002 | 0.2965 | 0.0394 | 0.0366 | 0.1312 | 0.1234 |
| $\tilde{\Omega}$ = 0.6, $M$ = 0.5 | 0.2993 | 0.2936 | 0.0605 | 0.0566 | 0.2021 | 0.1928 |
| $\tilde{\Omega}$ = 0.6, $M$ = 0.6 | 0.2983 | 0.2899 | 0.0792 | 0.0734 | 0.2655 | 0.2532 |
| $\tilde{\Omega}$ = 0.8, $M$ = 0.4 | 0.4016 | 0.3962 | 0.0673 | 0.0648 | 0.1676 | 0.1636 |
| $\tilde{\Omega}$ = 0.8, $M$ = 0.5 | 0.4000 | 0.3922 | 0.0914 | 0.0874 | 0.2285 | 0.2228 |
| $\tilde{\Omega}$ = 0.8, $M$ = 0.6 | 0.3986 | 0.3873 | 0.1144 | 0.108 | 0.2870 | 0.2789 |
| $\tilde{\Omega}$ = 1.2, $M$ = 0.4 | 0.6068 | 0.5991 | 0.1168 | 0.1139 | 0.1925 | 0.1901 |
| $\tilde{\Omega}$ = 1.2, $M$ = 0.5 | 0.6051 | 0.5931 | 0.1508 | 0.1455 | 0.2492 | 0.2453 |
| $\tilde{\Omega}$ = 1.2, $M$ = 0.6 | 0.6031 | 0.5856 | 0.1844 | 0.1755 | 0.3058 | 0.2997 |

We developed realistic modeling of a DTL, based on eq.(3.25), as well as an approximate treatment, according to eqs. (4.7) and (4.8). This approximation gives good insight into the behavior of the DTL for relatively large values of the parameter $\tilde{\Omega}$, as seen in Table 4.1. From this table, we can appreciate that $\bar{\beta}a$ is well given by the approximation $\tilde{\Omega}/2$ [see eq. (4.11)] regardless of the modulation $M$. On the other hand, in the last two columns, another rough approximation, $\Delta\beta/\bar{\beta} \simeq M/2$ [eq. (4.13)] is only reasonable for $\tilde{\Omega}$= 0.8 and 1.2. This is due to the fact that resistances are neglected in eqs. (4.11-13), and as $\Omega$ (and, therefore $\tilde{\Omega}$) increase, losses become less important [see eq. (4.15)]. Regarding the comparison between accurate and approximate solutions, this is quite good for $\tilde{\Omega}$= 0.6, 0.8 and 1.2, but fails for $\tilde{\Omega}$= 0.4 (even though both solutions take into account losses). The reason for this is that in eq. (4.8) the factor $(1+4R^2/\Omega^2L^2)^{1/2}$ was approximate by 1.

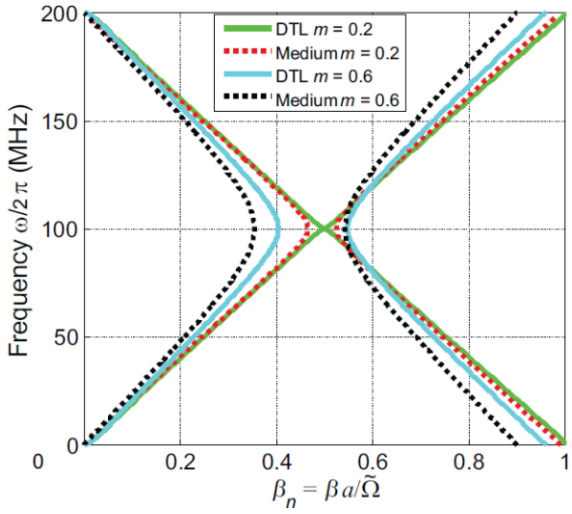


Figure 4.5. Band structures are compared for the DTL and the effective medium for two values of the modulation $m$. Band gaps are larger for the effective medium due to neglect of losses. The parameters are $R_\Omega$ = 2000 ohms, $G$ = 0.001 mhos, $R$ = 0.04 ohms, $\bar{V}_\Omega$ = 0.6 volts, $\Omega/2\pi$ = 200 MHz, and $\tilde{\Omega}$ = 0.53.

Now we compare the dispersion relations for the DTL and the effective medium. Because losses have not considered for the effective medium there is no a good agreement for the band-gap width. Fig. 4.5 shows the dispersion relations for two values of $m$, with the phase advance replaced by $\beta_n = \beta a/\tilde{\Omega}$. Taking into account the eqs. (3.30), $\beta_n = \beta/\Omega(\mu\bar{\varepsilon})^{1/2}$ for the effective medium is independent of the period $a$, as it should be. Fig. 4.6 presents the DTL and effective medium dispersion relations for three values of $\tilde{\Omega}$. There is a very good correspondence for values of the normalized phase advance $\beta_n$ smaller than about 0.5.

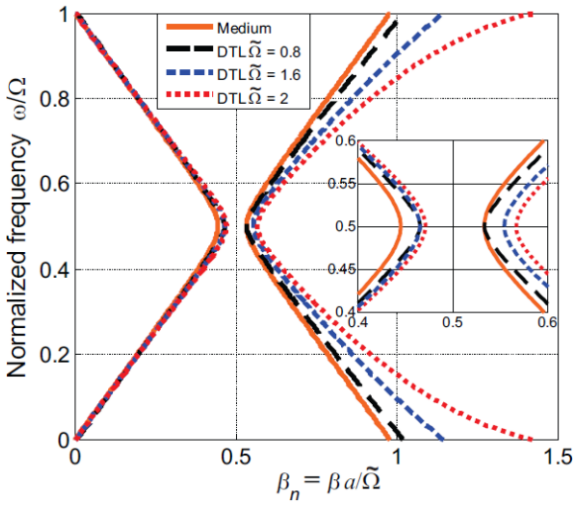


Figure 4.6. Dispersion curves for the DTL and effective medium for three values of the normalized circular frequency $\tilde{\Omega}$. Here $R_\Omega$ = 2000 ohms, $G$ = 0.001 mhos, $R$ = 0.04 ohms, $\bar{V}_\Omega$ = 0.6 volts, and $m$ = 0.3.

## 4.3. Experiment, experimental results, and comparison of experimental and theoretical band structures

First we discuss the components needed for the experiment. A DTL with eight 5mm cells was fabricated using microstrip technology on a RT Duroid

5880 substrate with the following characteristics: Dielectric constant = 2.2 ±0.02, dissipation factor (tan δ) = 0.0009, dielectric thickness = 1.575 mm, copper layer thickness = 35 μm. Commercial inductors of 1 mm x 0.5 mm were inserted in the DTL, with inductance of 10 nF in the internal cells and of 5 nF in the cells at the ends. A SMV1249 hyperabrupt union varactor from Skywoks of 1.6 mm x 0.8 mm was inserted in each cell. The voltage-capacitance relation for this varactor is shown in Fig. 2.2. There are seven vias of 0.5 mm to ground at each varactor ground level to guarantee good grounding. Besides the DTL, we also used: 1) Eight band-pass filters with central frequency of 310 MHz and fractional bandwidth of 5.6%. Each band-pass filter is based on a miniaturized ring resonator [30] of 16 mm x 16 mm fabricated on a RT Duroid 6010.2LM substrate with dielectric constant = 10.7, tan δ = 0.0023, and dielectric thickness = 1.27 mm. 2) Eight matched amplifiers with a RFMD's InGaP HBT MMIC amplifier using coplanar technology. 3) Two 50-ohm coaxial power splitters 4 way-0° ZN4PD1-63W+. 4) Two 50-ohm coaxial power splitters 2 way-0° ZX10R-14+. 5) Four low-pass filters with cutoff frequency of 260 MHz. 6) Low-loss 50-ohm coaxial cables. Fig. 4.7 shows a photograph of the fabricated DTL. More details of the fabricated components are shown in Appendix B.

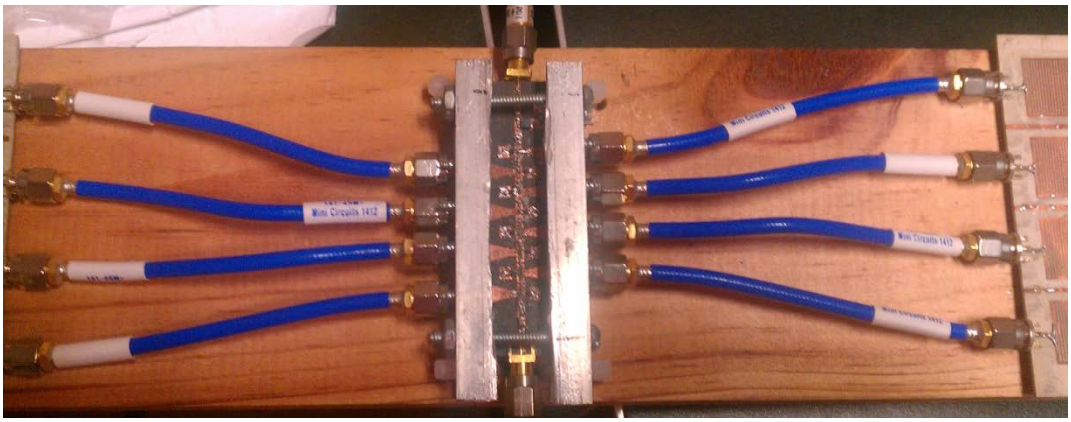

Figure 4.7. Photograph of the 63 mm x 25.2 mm fabricated 8-cell DTL, including feeding lines, ac blocking network, dc blocking capacitors and coupling impedances for the modulation lines. SMA connectors were used.

The experimental setup was as follows. The dc inverse polarization voltage was provided by a single dc voltage source through an ac blocking network. The modulation voltage signal of 310 MHz was obtained from a signal generator Anritsu MG3692C and then, with the combination of one 2-way splitter and two 4-way splitters, divided into eight equal voltage signals. Every divided signal then passed through the amplifiers and was amplified. In continuation, each of these signals went through a band-pass filter and then applied at each cell varactor in order to be modulated. A low-pass filter, used to filter the 310 MHz modulation voltage and higher frequency harmonics, was placed at each end of the DTL. The travelling wave signal of frequency $\omega/2\pi$ was generated from a signal generator Anritsu MG3696B and then divided by a 2-way splitter into two halves. One half went right through the DTL and the other half went from end to end of a transmission line with identical connectors, feeding lines, dc blocking capacitors, ac blocking network, and low-pass filters at its ends as the DTL. The two signals were then recovered, displayed, and stored on a 2.5 GHz LeCroy oscilloscope. Digital signal processing was then performed on the stored signals allowing them to be separated into individual wavelength components ($\beta_1 a$, $\beta_2 a$, …). After comparing both halved waves, the corresponding phase advance is obtained. The process is then repeated for different values of $\omega/2\pi$ (from 10 to 305 MHz) and the dispersion relation is gotten. The measurement schematic is shown in Appendix C.

The resulting experimental dispersion relation for voltage modulation of $m = 0.43$ and $m = 0.52$ for the normalized phase advance $\beta_n = \beta a/\tilde{\Omega}$ $\left[= \beta/\Omega(\mu\bar{\varepsilon})^{1/2}\right]$ are shown in Figs. 8(a) and (b). They are compared with the band structures obtained from “realistic theory” of the DTL (sec. 4.2) and the effective medium treatment (sec. 3.4). There is an excellent agreement between the three descriptions. As expected, the band gap increases with the modulation $m$ as we have already seen in Figs. 4.2 and 4.5. The dispersion

curves for the effective medium, though, become less and less accurate as $\beta_n$ increases beyond ~ 0.8, as in Fig. 4.5 and 4.6.

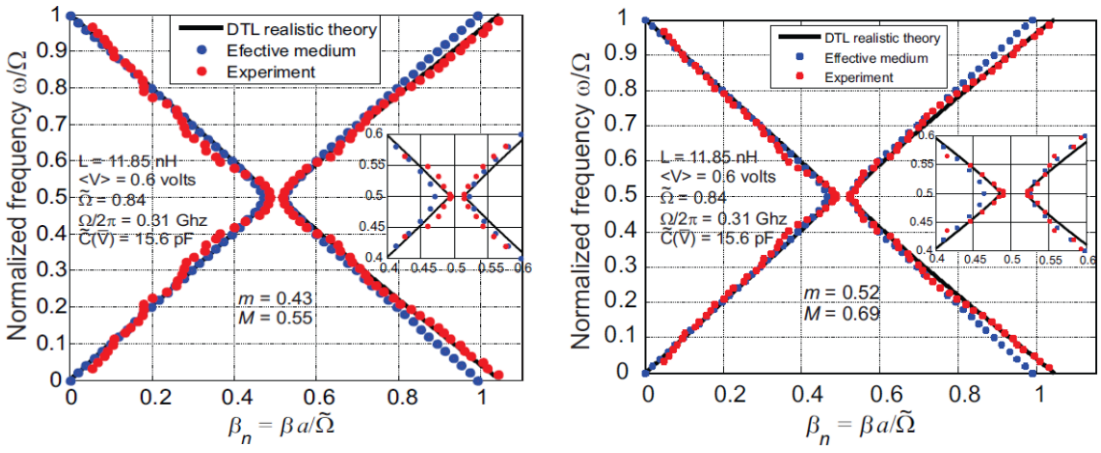


(a) (b)

Figure 4.8. Theoretical (black solid line) and experimental (red dots) dispersion relations, along with that for the corresponding effective medium (blue dots) for (a) $m$ = 0.43 and (b) $m$ = 0.52. An inset zooms in on the forbidden phase constant band. Such a gap in $\beta$-bands obtains only if $m > m_{min}$ = 0.39, see eq. (6.14 and 6.15).

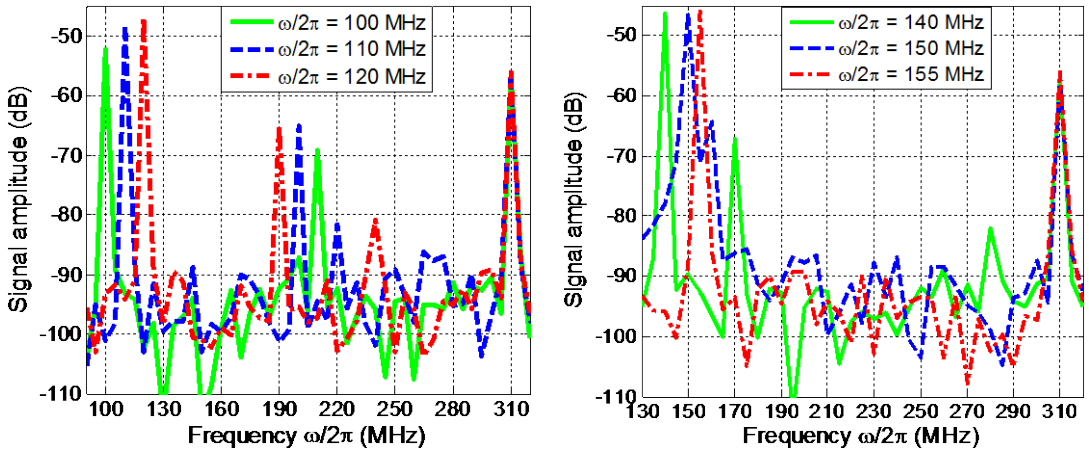


(a) (b)

Figure 4.9. Spectra of the recovered signals at the end of the DTL for six externally launched voltage signals of varying frequencies $\omega/2\pi$, where harmonics $(\Omega - \omega)/2\pi$ are also present. The peaks at $\Omega/2\pi$ = 310 MHz all have the same amplitude confirming that the modulation intensity is the same for all the externally launched signal frequencies and that the modulation voltage at all the nodes is the same $V_\Omega(t)$ as explained in the Appendix A. Here $L$ = 11.85 nH, $G$ = 0.001 mhos, $\bar{V}_\Omega$ = 0.6 volts, and $m$ = 0.5.

Figure 4.9 illustrates the measured spectra of several signals transmitted all the way through the DTL for the externally launched traveling waves of frequency $\omega/2\pi$ where the harmonics $(\Omega - \omega)/2\pi$ are present. The frequencies of the harmonics are: 210 MHz = (310 −100 MHz), 200 MHz = (310 − 110 MHz), 190 MHz = (310 − 120 MHz), 170 MHz = (310 − 140 MHz), and 160 MHz = (310 − 150 MHz).

In continuation, we present another experimental result for our fabricated DTL. As is well known, when two frequencies $\omega_1$ and $\omega_2$ are nearly equal to each other, beats occur [31]. This phenomenon can be observed in many cases being especially notable for sound. It follows from eq. (3.22) that a DTL has harmonics $(\omega - n\Omega)/2\pi$ due to temporal periodicity, as also described for a dynamic medium slab in ref. [26]. For the externally launched traveling wave signal of frequency $\omega_1$, the DTL generates another wave signal of frequency $\omega_2 = \Omega - \omega_1$. Figure 4.10 presents the interaction of these two signals for four cases of $\omega_1$ where beats can be appreciated. The beats of Fig. 4.10(a) have a frequency of 2 MHz corresponding to $|\omega_1 - \omega_2|/2\pi$ = |154 −156 MHz|. The beats of Figs. 4.10(b-d) have frequencies: |153 −157 MHz| = 4 MHz, |152 −158 MHz| = 6 MHz, and |150 −160 MHz| = 10 MHz. These values correspond to a modulation frequency of $\Omega/2\pi$ = 310 MHz, and modulation $m$ = 0.25.

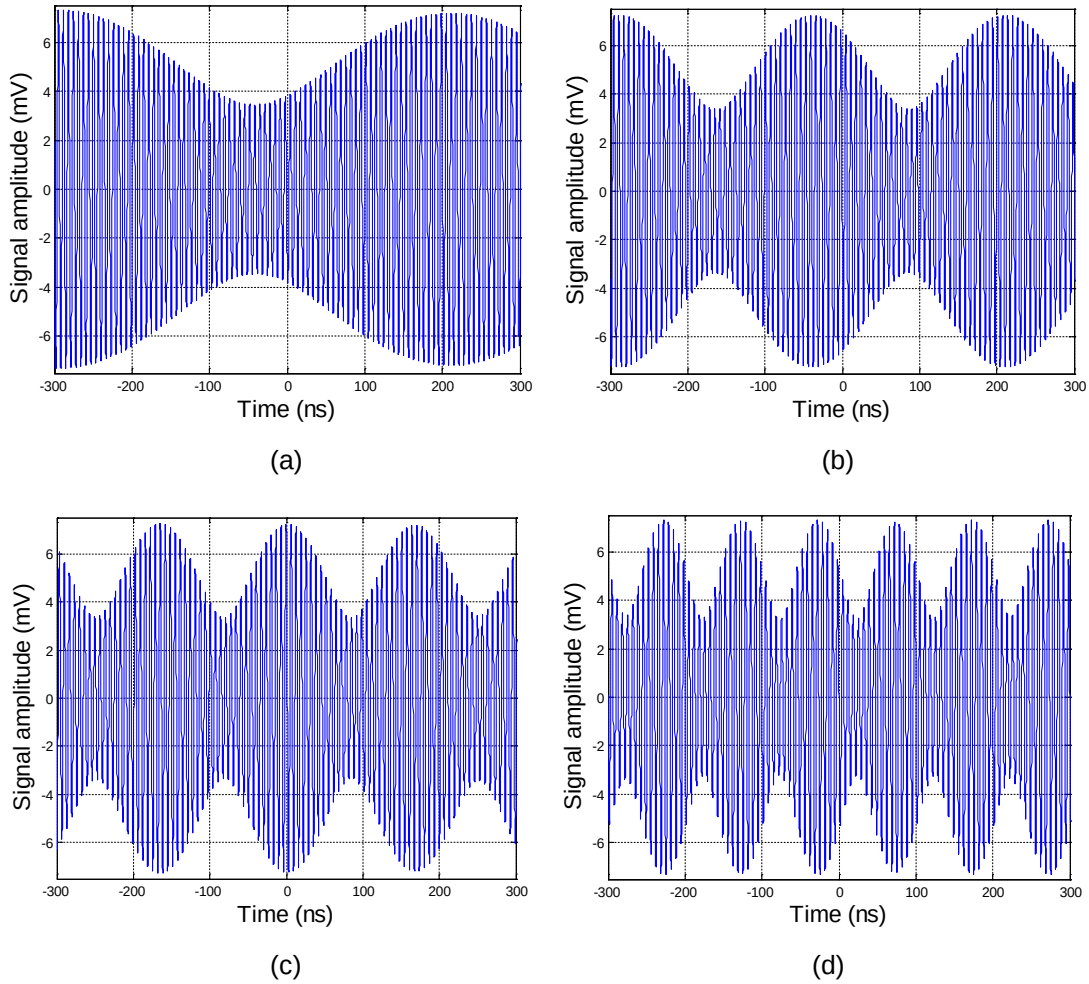


Figure 4.10. Recovered signals at the end of the DTL after digital signal processing where there is an envelope signal of lower frequency, corresponding to beats. The externally launched traveling waves have frequencies (a) 154 MHz, (b) 153 MHz, (c) 152 MHz, (d) and 150 MHz. Here $L$ = 11.85 nH, $G$ = 0.001 mhos, and $\overline{V}_{\Omega}$ = 0.3 volts.

# Chapter V

## Conclusions

We have presented an in-depth study of electromagnetic wave propagation in a low-pass DTL, with the capacitors replaced by varactors that are modulated identically by an external voltage source that is periodic in time. We have designed and fabricated such a DTL with a frequency of modulation $\Omega/2\pi$ = 310 MHz of the varactors. A series of signal waves with frequencies $\omega/2\pi$ up to 310 MHz were launched and the corresponding propagation constants $\beta(\omega)$ were measured. Two bands, $\beta_1(\omega)$ and $\beta_2(\omega)$, were obtained and these turn out to be separated by a band-gap $\Delta\beta$, provided that the modulation $M$ of the dynamic capacitances $\tilde{C}(t)$ is sufficiently strong to overcome resistive effects ($M > M_R$). This behavior is very well confirmed by a detailed calculation, based on the Bloch-Floquet theorem in time and applied to an accurate model of the DTL. Just as frequency gaps are characteristic of spatial periodicity, $\beta$-gaps are a hallmark of temporal periodicity. We believe that these are the first measurements of a forbidden band of the propagation constant $\beta$ (or wave vector $k$).

We also showed that for waves of sufficiently large wavelength in comparison to the cell size of the DTL ($\beta a \lesssim 1$) the dispersion $\beta(\omega)$ can be well represented by a mean-field theory. This, provided that the permittivity $\varepsilon(t)$ of the effective medium is equal to the distributed capacitance $\tilde{C}(t)/a$ at every instant of time and that the permeability $\mu$ of this medium is equal to the distributed inductance $L/a$, and neglecting damping effects. If these conditions are satisfied, then the dispersion relations in the effective medium and the DTL are identical. A dynamic effective medium is, actually, a "temporal photonic crystal", shown some years ago [26] to exhibit a forbidden band of its wave vector $k$, as well as other interesting features [27]. Thus, the present

work establishes a strong connection to dielectric media characterized by parameters that vary periodically in time.

We also demonstrated experimentally that, for every working frequency $\omega$ our DTL generates harmonics $(\Omega - \omega)/2\pi$ that correspond to the harmonics described for a dynamic medium in ref. [26]. In addition, we showed experimentally that our DTL generates beats for externally launched voltage signals of frequencies nearly equal to half of the modulation frequency.

A more detailed study of the propagation constant reveals the possibility of lossless transmission for the DTL (with vanishing attenuation constant $\alpha$) and is being prepared for future publication. Also, there is still need of experimental verification for different frequency ranges as well as for different parameters (such as $\tilde{\Omega}$) of the DTL. Split ring resonators with varactors fixed in the ring slots could lead to higher frequency ranges. Analog filtering and routing of a modulated signal by means of the same process would be also possible with the fabrication of a two-dimensional DTL.

Considering that we can control our DTL's impedance, frequency range, phase advance, and harmonic frequency values, some possible applications are: *parametric amplifiers*; *frequency converters* where the converted frequency can be smaller or larger than the original frequency; *controllable time-delay lines* with a large range; *frequency generators* where many frequency values can be obtained at the same time; *controllable filters* not only for the frequency value but for the phase advance value; *electronic prisms* a two-dimensional DTL could separate different frequency waves of a composed signal as a prism does to light; *controllable antennas* where not only the load impedance seen by the antenna can be controlled but the advance phase of the signal received by the antenna; and other applications associated with the abovementioned characteristics.

# Appendix A

For the low-pass DTL shown in Fig. 3.1, when the traveling wave of frequency $\omega$ is *not* present, the voltage at every node is the same, so that no current flows through the inductors. This voltage is given by a voltage divider where the capacitance $C[V(t)]$ and the conductance $G$ are in parallel. The resulting impedance is given by

$$Z_P = \frac{G + i\Omega C(V_N)}{i\Omega G C(V_N)}. \qquad \text{(A.1)}$$

The voltage at the node is

$$V_N = \frac{V_\Omega \left[G + i\Omega C(V_N)\right] / i\Omega G C(V_N)}{R_\Omega + \left[G + i\Omega C(V_N)\right] / i\Omega G C(V_N)}. \qquad \text{(A.2)}$$

This equation can be rewritten as

$$V_N = \frac{V_\Omega \left[G + i\Omega C(V_N)\right]}{G + i\Omega C(V_N)\left[1 + R_\Omega G\right]}. \qquad \text{(A.3)}$$

The resistance $R_\Omega$ is frequency dependant: $R = R_\Omega(\omega)$. It has a very low value at the frequency $\Omega$, i.e., the traveling wave of frequency $\omega$ "sees" a very high resistance value, whereas the modulation signal of frequency $\Omega$ experiences a very low resistance value. This can be achieved with the specific physical length of a resonator. Since $R_\Omega(\Omega)G << 1$, eq. (A.3) becomes

$$V_N(t) \cong V_\Omega(t). \qquad \text{(A.4)}$$

The voltage at every node is mostly given by $V_\Omega(t)$ independently of the frequency $\omega$ of the traveling wave (excluding frequencies $\cong \Omega$). This can be also seen in Fig. 4.9 where all the peaks at $\Omega/2\pi$ = 310 MHz have the same amplitude, regardless of the frequency value $\omega$ of the externally launched traveling waves.

# Appendix B

In this section the layouts of the fabricated circuits are shown along with the frequency response of the band-pass filter.

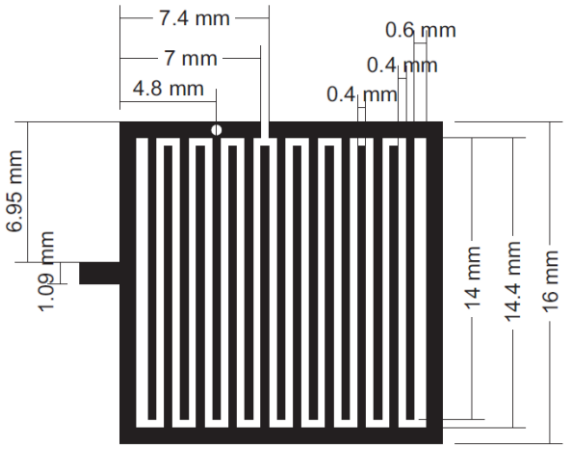


Figure B.1. Layout of the ring resonator used in the band-pass filters where each gap is of 0.4 mm but with the exception of the horizontal ends which are 0.6 mm. The ring resonator has a gap and a via to ground (white circle) in order to reduce its size.

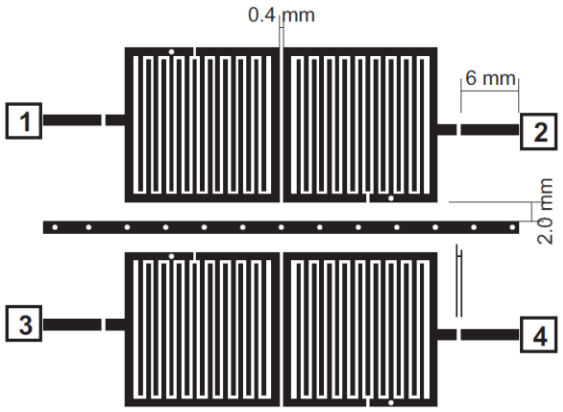


Figure B.2. Layout of two contiguous band-pass filters where a line with various vias to ground is placed between the filters in order to reduce crosstalk. The gap at the 50-ohm-feeding lines where dc blocking capacitor is placed is also shown.

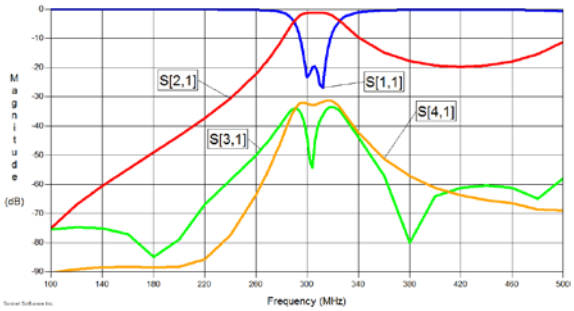


Figure B.3. S-parameters for the circuit shown in Fig. B.2. The band pass with central frequency at 310 MHz can be appreciated as well as the crosstalk which is below 30 dB for all frequencies.

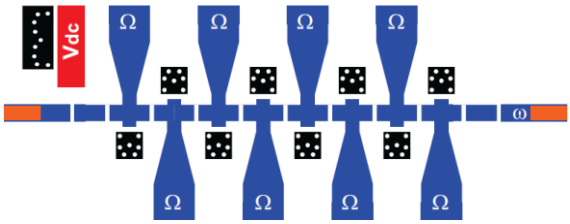


Figure B.4. Layout of the fabricated DTL, the places where the modulation voltage signal is applied are indicated for the symbol Ω, the place where the traveling voltage signal is applied is indicated for the symbol $\omega$. The dc level is indicated by Vdc. The black segments represent the grounded levels; all of them have vias to ground of 0.5 mm.

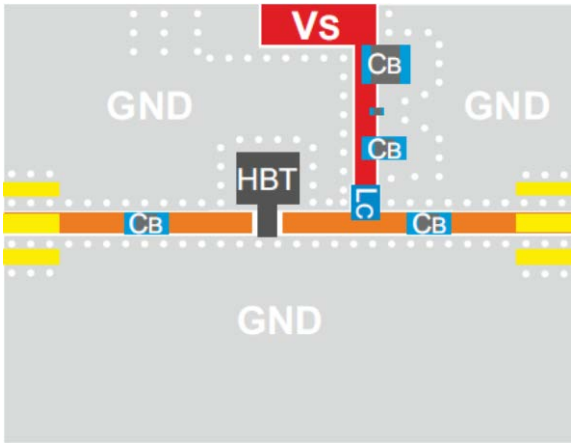


Figure B.5. Layout of the fabricated amplifier using 50 ohms coplanar lines, the width of the gaps is 0.25 mm, the coupling inductor is denoted by $L_C$, and the blocking capacitors are denoted by $C_B$. All the grey sections are grounded levels. The red section is the dc level.

# Appendix C

In this appendix we present the used measurement schematic.

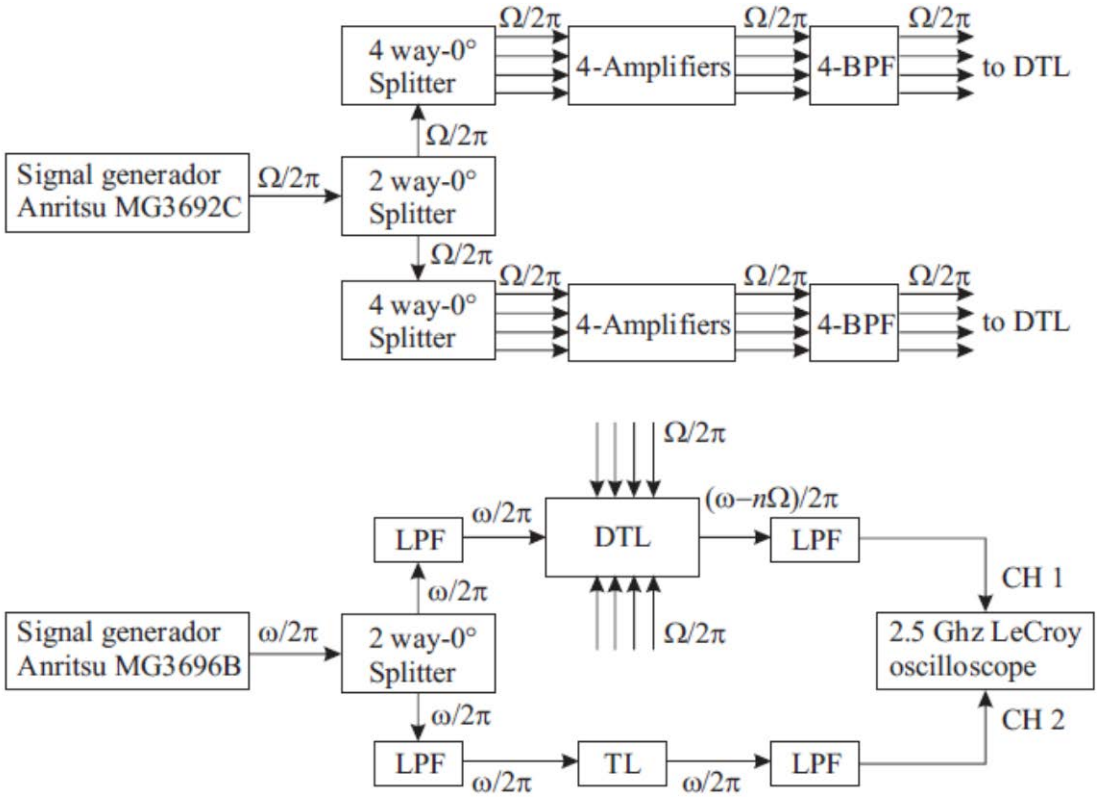


Figure C.1. Schematic used for the measurement where: LPF indicates low-pass filter, BPF means band-pass filter, CH stand for oscilloscope channel and TL includes feeding lines, ac blocking network, blocking capacitors and connectors that are also present at the DTL.

# Figure index

# Table index

# References


[1] A. L. Cullen, “A traveling wave parametric amplifier,” *Nature*, vol.**181** no.4605, p.332, February, 1958. doi:10.1038/181332a0

[2] A. L. Cullen, “Theory of the traveling-wave parametric amplifier,” *Proceedings of the IEE – Part B: Electronic and Communication Engineering*, vol.**107** no.32, p.101,107, March, 1960. doi: 10.1049/pi-b-2.1960.0085

[3] P. K. Tien and H. Suhl, "A Traveling-Wave Ferromagnetic Amplifier," *Proceedings of the IRE* , vol.**46**, no.4, pp.700,706, April, 1958. doi: 10.1109/JRPROC.1958.286770

[4] P. K. Tien, "Parametric amplification and frequency mixing in propagating circuits," *J. Appl. Phys.*, vol.**29**, no.9, pp.1347,1357, September, 1958. doi: http://dx.doi.org/10.1063/1.1723440

[5] A. Ashkin, T.J. Bridges, W.H. Lousell, and C.F. Quate, "Parametric amplification of space-charge waves," *Proceedings of the IEE - Part B: Radio and Electronic Engineering* , vol.**105**, no.11, pp.649,651, May 1958. doi: 10.1049/pi-b-1.1958.0140

[6] G.M Roe, M.R. Boyd, "Parametric Energy Conversion in Distributed Systems," *Proceedings of the IRE*, vol.**47**, no.7, pp.1213,1218, July 1959. doi: 10.1109/JRPROC.1959.287353

[7] C. Bell and G. Wade, "Iterative Traveling-Wave Parametric Amplifiers," *Circuit Theory, IRE Transactions on*, vol.**7**, no.1, pp.4,11, March, 1960. doi: 10.1109/TCT.1960.1086619

[8] R. C. Honey and E. M. T. Jones, “A Wide-Band UHF Traveling-Wave Variable Reactance Amplifier," *Microwave Theory and Techniques, IRE Transactions on*, vol.**8**, no.3, pp.351,361, May, 1960. doi: 10.1109/TMTT.1960.1125245

[9] M.R. Currie and R.W. Gould, "Coupled-Cavity Traveling-Wave Parametric Amplifiers: Part I-Analysis," *Proceedings of the IRE*, vol.**48**, no.12, pp.1960,1973, Dec. 1960. doi: 10.1109/JRPROC.1960.287564

[10] K.P. Grabowski and R.D. Weglein, "Coupled-Cavity Traveling-Wave Parametric Amplifiers: Part II-Experiments," *Proceedings of the IRE* , vol.**48**, no.12, pp.1973,1987, Dec. 1960 doi: 10.1109/JRPROC.1960.287565

[11] E.S. Cassedy, "Temporal Instabilities in Traveling-Wave Parametric Amplifiers (Correspondence)," *Microwave Theory and Techniques, IRE Transactions on*, vol.**10**, no.1, pp.86,87, January 1962. doi: 10.1109/TMTT.1962.1125452

[12] E.S. Cassedy and A.A. Oliner, "Dispersion relations in time-space periodic media: Part I—Stable interactions," *Proceedings of the IEEE*, vol.**51**, no.10, pp.1342,1359, Oct. 1963. doi: 10.1109/PROC.1963.2566

[13] E.S. Cassedy, "Dispersion relations in time-space periodic media part II—Unstable interactions," *Proceedings of the IEEE*, vol.**55**, no.7, pp.1154,1168, July 1967. doi: 10.1109/PROC.1967.5775

[14] E.S. Cassedy, "Waves guided by a boundary with time-space periodic modulation," *Electrical Engineers, Proceedings of the Institution of*, vol.**112**, no.2, pp.269,279, February 1965. doi: 10.1049/piee.1965.0040

[15] O.J. Downing and P.A. Watson, "Active and passive broadbanding of parametric amplifiers," *Electrical Engineers, Proceedings of the Institution of*, vol.120, no.**6**, pp.629,636, June 1973. doi: 10.1049/piee.1973.0138

[16] K. Inal and C. Toker, "Accurate Determination of Varactor Resistance at UHF and Its Relation to Parametric Amplifier Noise Temperature," *Microwave Theory and Techniques, IEEE Transactions on*, vol.**21**, no.5, pp.327,333, May 1973. doi: 10.1109/TMTT.1973.1127990

[17] J.J. Harris and J.M Woodcock, "Low noise GaAs varactor and mixer diodes prepared by molecular beam epitaxy," *Electronics Letters*, vol.**16**, no.9, pp.317,319, April 24 1980. doi: 10.1049/el:19800228

[18] R. Swartz, "Technology commentary - In perspective: The tunnel diode," *Solid-State Circuits Conference. Digest of Technical Papers. 1986 IEEE International*, vol.**XXIX**, pp.277,280, 19-21 Feb. 1986. doi: 10.1109/ISSCC.1986.1156891

[19] M.M. Driscoll, "Phase noise performance of analog frequency dividers," *Ultrasonics, Ferroelectrics, and Frequency Control, IEEE Transactions on*, vol.**37**, no.4, pp.295,301, July 1990. doi: 10.1109/58.56490

[20] A.-S. Porret, T. Melly, C.C. Enz, and E.A. Vittoz, "Design of high-Q varactors for low-power wireless applications using a standard CMOS process," *Solid-State Circuits, IEEE Journal of*, vol.**35**, no.3, pp.337,345, March 2000. doi: 10.1109/4.826815

[21] S. Ranganathan and Y. Tsividis, "Discrete-time parametric amplification based on a three-terminal MOS varactor: analysis and experimental results," *Solid-State Circuits, IEEE Journal of*, vol.**38**, no.**12**, pp.2087,2093, Dec. 2003. doi: 10.1109/JSSC.2003.819162

[22] Wooram Lee; E. Afshari, "Distributed parametric resonator: A passive CMOS frequency divider," *Solid-State Circuits, IEEE Journal of*, vol.**45**, no.9, pp.1834,1844, September, 2010. doi: 10.1109/JSSC.2010.2056833

[23] Wooram Lee; E. Afshari, "Low-Noise Parametric Resonant Amplifier," *Circuits and Systems I: Regular Papers, IEEE Transactions on*, vol.**58**, no.3, pp.479,492, March, 2011. doi: 10.1109/TCSI.2010.2072370

[24] Qin Shihan, Xu Qiang, and Y.E. Wang, "Nonreciprocal Components With Distributedly Modulated Capacitors," *Microwave Theory and Techniques, IEEE Transactions on*, vol.**62**, no.10, pp.2260,2272, Oct. 2014. doi: 10.1109/TMTT.2014.2347935

[25] P. Halevi, U. Algredo-Badillo, and J.R. Zurita-Sánchez, “Optical response of a slab with time-periodic dielectric function ε(t): towards a dynamic metamaterial,” *Proc. SPIE,* vol.**8095**, p.80950I, September, 2011. doi: 10.1117/12.892953

[26] J.R. Zurita-Sánchez, P. Halevi, and J.C. Cervantes-González, “Reflection and transmission of a wave incident on a slab with time-periodic function ε(t),” *Phys. Rev. A,* vol.**79**, no.5, p.053821, May, 2009. doi: http://dx.doi.org/10.1103/PhysRevA.79.0538

[27] J.R. Zurita-Sánchez and P. Halevi, “Resonances in the optical response of a slab with time-periodic dielectric function ε(t),” *Phys. Rev. A,* vol.**81**, no.5, p.053834 May, 2010. doi: http://dx.doi.org/10.1103/PhysRevA.81.053834

[28] J.R. Zurita-Sánchez, J.H. Abundis-Patiño, and P. Halevi, “Pulse propagation through a slab with time-periodic dielectric function ε(t),” *Opt. Express*, vol.**20**, no.5, pp.5586,5600, February, 2012. doi: 10.1364/OE.20.005586

[29] *Introduction to Solid State Physics*, 8th ed., John Wiley & Sons, Hoboken, NJ, 1985, pp. 176–180.

[30] J.R. Reyes-Ayona, M.Sc. thesis, Instituto Nacional de Astrofísica, Óptica y Electrónica, 2010.

[31] *Mechanical vibrations*, First ed., Dover Publications, New York, NY, 1985, pp. 5–7.

# Resumen en extenso

## Introducción.

En la década de los 60s del siglo pasado, los amplificadores paramétricas de onda viajera (APOV) fueron ampliamente estudiados teoréticamente. Los APOVs consisten en una línea de transmisión pasa-bajas en la cual cada una de sus celdas está formada por un inductor en serie y un capacitor con una conexión a tierra. Los capacitores de la línea de transmisión eran modelados en el espacio y en el tiempo por una onda viajera [1], o dos líneas acopladas eran embebidas en un medio ferro-magnético modulado [3]. Para el primer caso, se reporto la relación de dispersión de una línea de transmisión sin pérdidas [12]. Dos señales eran aplicadas a los APOVs en alguno de sus extremos: una que sería parametricamente amplificada y una señal de amplitud grande usada como señal de bombeo. La caída de voltaje que experimentaba cada capacitor variaba con la fase de la onda de bombeo viajera. Sin embargo, la ausencia de varactores de buena calidad dificulto la verificación experimental para las capacitancias moduladas. Recientemente, se simulo un amplificador paramétrico con varactores depositados en un proceso de CMOS [23].

Es bien sabido que en el límite de onda larga, una línea de transmisión puede ser descrita usando a un medio efectivo. Por esta razón, trabajos previos en medios dieléctricos que son modulados en el tiempo son altamente relevantes para el presente estudio. Se encontró que una permitividad periódicamente cambiante da lugar a bandas prohibidas en el avance de fase (en vez de la frecuencia) y a múltiples armónicos en la luz reflejada o transmitida por una placa con esta permitividad [26]. Condiciones geométricas especiales aplicadas a esta placa dan lugar a resonancias paramétricas [27]. Y que un pulso transmitido a través de una placa dinámica es separado en armónicos de la frecuencia de modulación y sus picos

pueden emerger al otro lado de la placa más rápido que la luz en el vacío [28]. Se espera que estas características de un medio dinámico también se obtengan para una línea de transmisión dinámica (LTD).

Presentamos un reporte experimental y teórico sobre LTDs cuyos capacitores son modelados en tándem, las capacitancias son idénticas en todas y cada una de las celdas en cualquier instante de tiempo por lo que nuestra LTD es cualitativamente diferente de los antes mencionados APOVs. A continuación se describe el proceso de modulación y se presenta un modelo realista para la LTD, esto seguido por una descripción de la fabricación y del experimento. Un modelo simplificado bosqueja el método teórico mientras que los resultados del modelo realista así como los de un medio efectivo son comparados con los experimentales.

## Modelo.

La modulación de nuestra LTD se logra por medio de varactores cuya capacitancia es controlada por una fuente de voltaje de ca, y una fuente de voltaje de cd es usada para polarizar inversamente al varactor. El voltaje aplicado a los varactores es $V_\Omega = \overline{V}_\Omega(1 + m \sin \Omega t)$, donde $\overline{V}_\Omega$ es el voltaje de polarización inversa, $\Omega/2\pi$ es la frecuencia de modulación y $m$ es la intensidad de la fuente de ca. Siendo la capacitancia dependiente del voltaje, la corriente está dada por $I(t) = (d/dt)[C(V)V(t)] \equiv \tilde{C}_{(V)}\, dV/dt$, donde $\tilde{C}_{(V)} = C(V) + C'(V)V$ con $C'(V) = dC/dV$. La capacitancia dinámica $\tilde{C}_{(V)}$ es apropiada para tratar con la LTD en lugar de la capacitancia ordinaria $C$. La Figura 1 compara sus dependencias correspondientes con el voltaje.

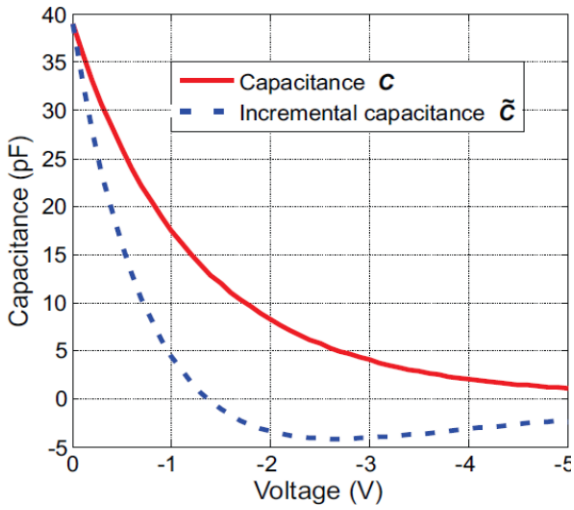


Figura 1. Capacitancias convencional y dinámica en función del voltaje aplicado para los diodos varactores de la LTD.

Además de la consideración de la fuente de voltaje $V_\Omega(t)$, una descripción realista de la LTD requiere una conductividad finita para las líneas de cobre de la microcinta modeladas como resistencia en serie $R$, las pérdidas de substrato modeladas como una conductancia con una conexión a tierra $G$, una corriente de fuga por las líneas de alimentación $R_\Omega$, y una capacitancia parasítica (que no se puede modular) debida a la microcinta. El valor de la resistencia $R_\Omega$ debe de ser alto para evitar flujo de corriente a través de la fuente de voltaje. La celda unitaria de la LTD se muestra en la Fig. 2 junto con las corrientes y voltajes asociados a los nodos $N$ y $N$+1.

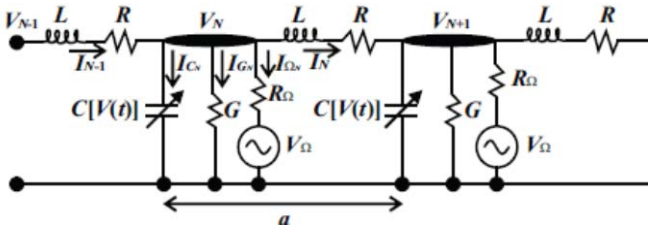


Figura. 2. Celda unitaria de la DTL de longitud *a* entre los nodos $N$ y $N+1$. Las capacitancias $\tilde{C}(t)$ son moduladas en tándem, es decir, los voltajes $V_\Omega$ tienen la misma amplitud y fase en todos los nodos. Esto da como resultado que la diferencia de voltaje $V_{N+1} - V_N$ sea dada solo por la (pequeña) señal de voltaje de frecuencia $\omega$ de la onda viajera.

## Experimento.

Se fabrico una línea de transmisión dinámica de ocho celdas, usando tecnología de microcinta, en un substrato RT Duroid 5880 con espesor de 1.575 mm. Cada celda tiene una longitud de 5 mm. Los varactores son diodos de unión híper-abrupta SMV1249 de Skyworks. La frecuencia del voltaje de modulación fue de 310 MHz y se obtuvo de un generador de señales Anritsu MG3692C. Esta señal de modulación se dividió en ocho señales de voltaje idénticas usando divisores de potencia. Cada señal de modulación se amplifico en un amplificador acoplado que se fabrico específicamente para ello. Estos amplificadores usan un transistor RFMD HBT MMIC de InGaP. Después de ser amplificada, cada señal pasa a través de un filtro pasa banda (basado en anillos resonadores y centrado a 310 MHz con un ancho fraccional de 5.6%) y entonces aplicada a cada varactor. El voltaje de polarización inversa provino de una sola fuente de voltaje de cd y paso por una red de bloqueo de ca. Se coloco un filtro pasa bajas en cada extremo de la LTD para filtrar a la señal de modulación de 310 MHz así como a los armónicos de frecuencias mayores a 310 MHz. La señal de onda viajera de frecuencia $\omega/2\pi$ fue obtenida de un generador de funciones Anritsu MG3696B y primeramente dividida en dos partes iguales por un divisor de potencia. Cada mitad siguió una trayectoria casi idéntica, la única diferencia es que una pasa a través de la LTD y la otra no. Las dos señales son recuperadas, desplegadas y almacenadas en un osciloscopio Lecroy de 2.5 GHz. Posteriormente, se realizo procesamiento digital a las señales almacenadas lo que permitió separarlas en componentes individuales de longitud de onda ($\beta_1 a$, $\beta_2 a$, …). Después de comparar ambas mitades recuperada y procesadas se obtuvo el avance de fase correspondiente. El proceso se repitió para diferentes valores de $\omega/2\pi$ (de 10 a 305 MHz) y así se obtuvo la relación de dispersión. La fotografía de la LTD fabricada se muestra en la Figura 3.

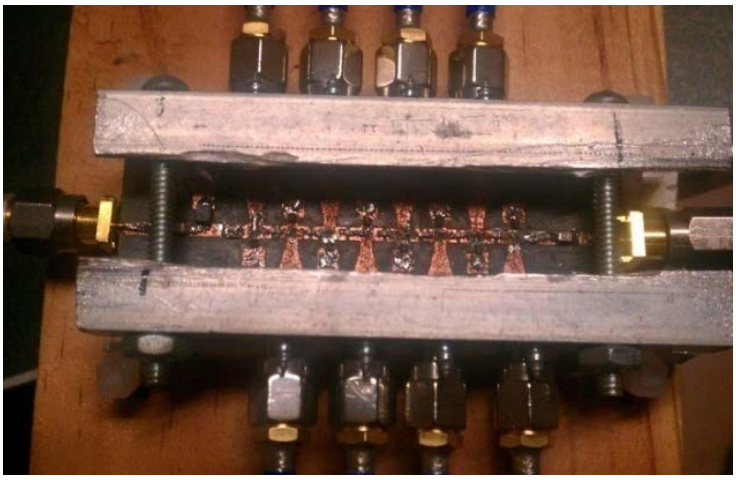

Figura 3. Fotografía de la LTD de ocho celdas fabricada. El tamaño total del circuito es de 63 mm x 25.2 mm, esto incluye a las líneas de alimentación, los capacitores de acoplamiento a cd y la red de bloqueo de ac. Cuatro señales de voltaje de modulación fueron aplicadas en cada lado de la LTD. Siete vías a tierra de 0.5 mm se colocaron en cada nivel de tierra de los varactores.

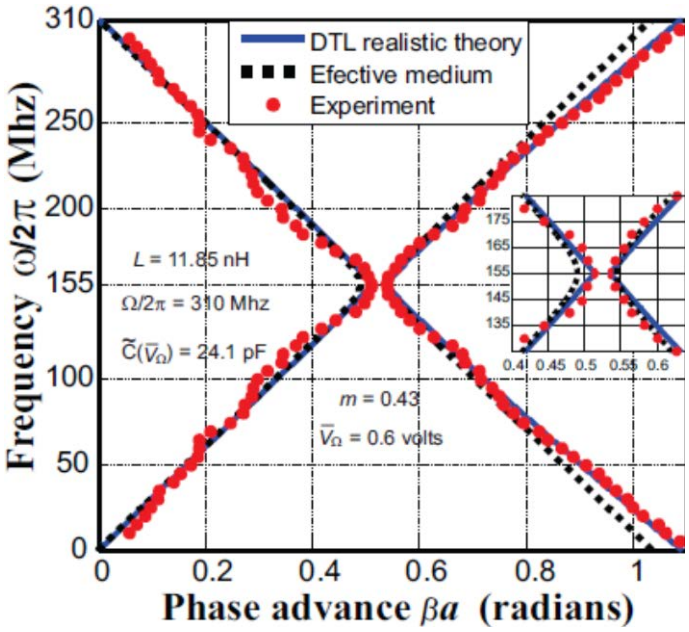


Figura 4. Relación de dispersión experimental (puntos rojos) y teórica (línea continua azul) de la LTD para una intensidad del voltaje de modulación de $m = 0.43$, junto con la relación de dispersión del medio efectivo (línea punteada negra). Un recuadro muestra la banda prohibida para el avance de fase. Dicha banda prohibida en $\beta$ solo se obtiene si $m > m_{min} = 0.39$.

La relación de dispersión experimental de la LTD para una intensidad de modulación $m = 0.43$ se muestra en la Fig. 4. Como se esperaba, hay una banda prohibida para la constante de fase $\beta$. La existencia y tamaño de la banda prohibida está directamente relacionada con $m$, la cual debe de ser lo suficientemente grande para superar a las pérdidas. Resulta que el valor de umbral de $m$ que da lugar a bandas prohibidas en $\beta$ es:

$$m_{min} = 4\left(R\tilde{C}/L + G + 1/R_{\Omega}\right)\Big/\tilde{C}'\overline{V}_{\Omega}\Omega\,. \qquad (1)$$

Dicha banda prohibida es una consecuencia de la periodicidad temporal, así como las bandas prohibidas en $\omega$ son causadas por la periodicidad espacial.

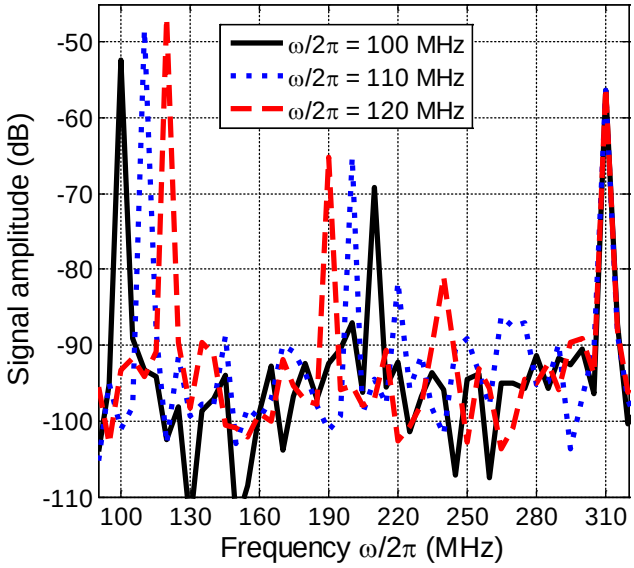


Figura 5. Espectros de las tres señales de voltaje externamente aplicadas de frecuencia $\omega/2\pi$ y transmitidas por la LTD. La línea solida (negra) es la de una señal aplicada de 100 MHz y tiene un armónico en 210 MHz (= 310 – 100 MHz). La línea punteada (azul) es la de una señal aplicada de 110 MHz y tiene un armónico en 200 MHz (= 310 – 110 MHz). La línea discontinua (roja) es la de una señal aplicada de 120 MHz y tiene un armónico en 190 MHz (= 310 – 120 MHz).

Para describir mejor a la LTD, se aplica la Transformada Rápida de Fourier a las señales de voltaje transmitidas por la LTD (después de las ocho celdas). La Figura 5 muestra los espectros de tres señales de frecuencias $\omega/2\pi$ = 100, 110, and 120 MHz. Como se puede apreciar, las señales transmitidas contienen armónicos $|\omega - n\Omega|/2\pi$ de la frecuencia de modulación, como deberían de tener. El pico a 310 MHz se puede apreciar que es idéntico para las tres señales $\omega$, como se esperaba. Sin embargo, debido al filtro pasa-bajas este pico es tres órdenes de magnitud menor de lo que es dentro de la LTD e incluso si fuera del mismo orden de magnitud que los picos de $\omega$, las diferentes componentes de $\omega$ se pueden separar fácilmente usando procesamiento digital. La Figura 6 muestra los golpecitos de frecuencia obtenidos para señales transmitidas de frecuencia $\omega/2\pi$ = 154 y 153 MHz. Mientras que en la Figura 7 se muestran para $\omega/2\pi$ = 152 y 150 MHz. Los golpecitos de la Figura 6(a) son de una frecuencia de 2 MHz, lo cual corresponde a $|\omega_1 - \omega_2|/2\pi$ = |154 −156 MHz|. Para la Figura 6(b) son |153 −157 MHz| = 4 MHz. En la figura 7 son |152 −158 MHz| = 6 MHz, y |150 −160 MHz| = 10 MHz.

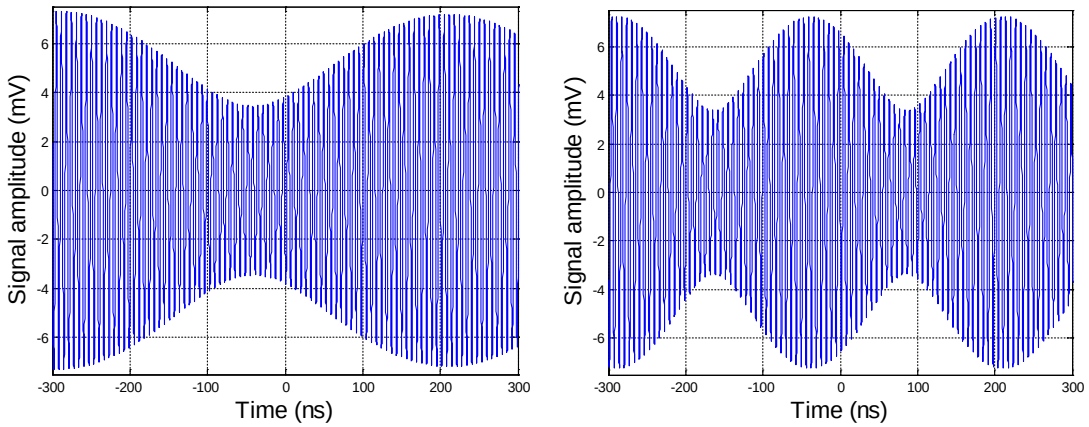


(a) (b)

Figura 6. Señales recuperadas al final de la LTD después de aplicar procesamiento digital donde se aprecia a una envolvente de frecuencia baja para las señales de onda viajera externamente aplicadas de frecuencia (a) 154 MHz, y (b) 153 MHz.

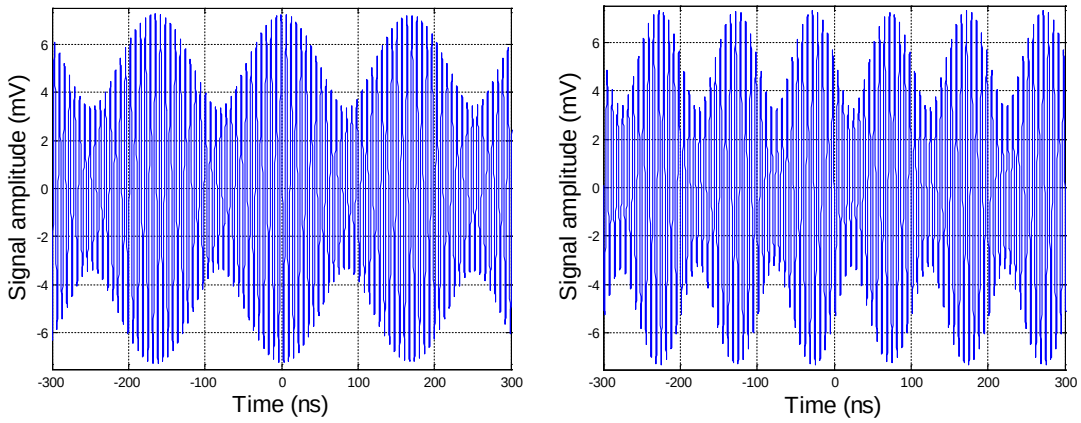


(a) (b)

Figura 7. Señales recuperadas al final de la LTD después de aplicar procesamiento digital donde se aprecia a una envolvente de frecuencia baja para las señales de onda viajera externamente aplicadas de frecuencia (a) 152 MHz, (b) y 150 MHz.

## Teoría.

Para tener una idea del comportamiento de las ondas que se propagan en la LTD, despreciamos a la resistencia $R$ y a la conductancia $G$, también asumimos que la resistencia $R_\Omega$ es tan larga que virtualmente no hay flujo de corriente a través de ella. De esta manera las caídas de voltaje $V_{N\text{-}1} - V_N$ y $V_N - V_{N+1}$ están dadas respectivamente por $LdI_{N\text{-}1}/dt$ y $LdI_N/dt$. Usando la ley de corrientes de Kirchhoff en el nodo $N$ de la Figura 2, resulta que

$$L\frac{d\left(I_{N-1}-I_N\right)}{dt}=L\frac{dI_{C_N}}{dt}=\left(V_{N-1}-V_N\right)-\left(V_N-V_{N+1}\right) \qquad (2).$$

Como se explico anteriormente, la corriente que fluye por el varactor es $I_{C_N}=\tilde{C}(V)dV/dt$ . El voltaje nodal $V_N$ está compuesto por el voltaje $V_\Omega$ que alimenta al varactor y la (mucho más pequeña) onda de señal que se propaga hacia la derecha:

$$V_N(t) = V_\Omega(t) + v(t)e^{i\beta aN} \tag{3}$$

Por consiguiente, la ecuación previa se reduce a

$$L\frac{d}{dt}\left\{\tilde{C}[V_N(t)]\frac{dV_N}{dt}\right\} = \left(e^{-i\beta a} + e^{i\beta a} - 2\right)v(t)e^{i\beta aN} \tag{4}$$

En la parte encerrada por llaves se ignoran los términos que son proporcionales a $V_\Omega$ debido a que nos interesa la onda preparatoria y no la fuente de modulación (la cual es idéntica en todas las celdas). Despreciando los términos proporcionales a $v^2$, la última ecuación se vuelve

$$\tilde{C}[V_\Omega(t)]\frac{d^2v}{dt^2} + 2\frac{d\tilde{C}}{dV_\Omega}\frac{dV_\Omega}{dt}\frac{dv}{dt} + \left[\frac{d}{dt}\left(\frac{d\tilde{C}}{dV_\Omega}\frac{dV_\Omega}{dt}\right) + \frac{4}{L}\sin^2\left(\frac{1}{2}\beta a\right)\right]v(t) = 0 \tag{5}$$

Se hace una aproximación para el varactor por el siguiente modelo lineal $\tilde{C}(V_\Omega) = \tilde{C} + \tilde{C}(V_\Omega - \overline{V}_\Omega) = \tilde{C}'\overline{V}m\sin(\Omega t)$ y la ecuación diferencial se simplifica a

$$\begin{aligned}\left[\tilde{C} + \tilde{C}'\overline{V}_\Omega m\sin(\Omega t)\right]\frac{d^2v}{dt^2} + \tilde{C}'\overline{V}_\Omega m\Omega\cos(\Omega t)\frac{dv}{dt} \\ + \left[(4/L)\sin^2(\beta a/2) - \tilde{C}'\overline{V}_\Omega m\Omega^2\sin(\Omega t)\right]v(t) = 0\end{aligned} \tag{6}$$

Ya que los coeficientes son periódicos en el tiempo, la solución tiene la forma $v(t) = \sum_n v_n \exp[i(n\Omega - \omega)t]$ que conlleva a un problema de eigenvalores para los coeficientes Fourier $v_n$. La ecuación (6) fue generalizada para la no linealidad de  y para las pérdidas, de acuerdo al modelo de la Figura 2. Los eigenvalores $\omega(\beta)$ obtenidos de esta teoría realista son trazados en la Figura. 4 (línea azul continua) mostrando una excelente correspondencia para las dos bandas experimentales $\beta$ (puntos rojos).

En el límite de onda larga $2\pi/k >> a$ una línea de transmisión sin perdidas puede ser descrita por un medio efectivo en el cual las ondas electromagnéticas obedecen la misma relación de dispersión $\omega(\beta)$. Dicho medio es definido por una permitividad efectiva $\varepsilon(t) = \tilde{C}(t)/a$ y una

permeabilidad efectiva $\mu = L/a$. La relación de dispersión para el medio efectivo es trazada en la Figura 4 por medio de puntos negros. Hay un excelente ajuste entre las curvas teóricas y experimentales para $\beta a < \pi/4$, con la excepción de la región de cuello de botella que es demasiado sensible para la omisión de la absorción.

## Conclusiones.

Se desarrollo una teoría generalizada para la línea de transmisión dinámica al igual que una teoría aproximada que resulta en una solución analítica la cual da una idea del comportamiento de las ondas transmitidas por la LTD. Se probó que la LTD se puede describir a través de un medio efectivo. Se probo que la LTD genera armónicos $(\Omega - \omega)/2\pi$ los cuales corresponden a los armónicos descritos para un medio dinámico [26]. Además se mostro que la LTD genera golpecitos en frecuencia para señales de voltaje externamente aplicadas cuya frecuencia es próxima a la mitad de la frecuencia de modulación.